Monte Carlo methods in critical systems

Catarina Martins Cosme
Mestrado em Física
Departamento de Física e Astronomia
2013/2014

Orientador
Dr. João Miguel Augusto Penedones Fernandes, Investigador auxiliar, FCUP

Coorientador
Dr. João Manuel Viana Parente Lopes, Professor auxiliar convidado, FCUP

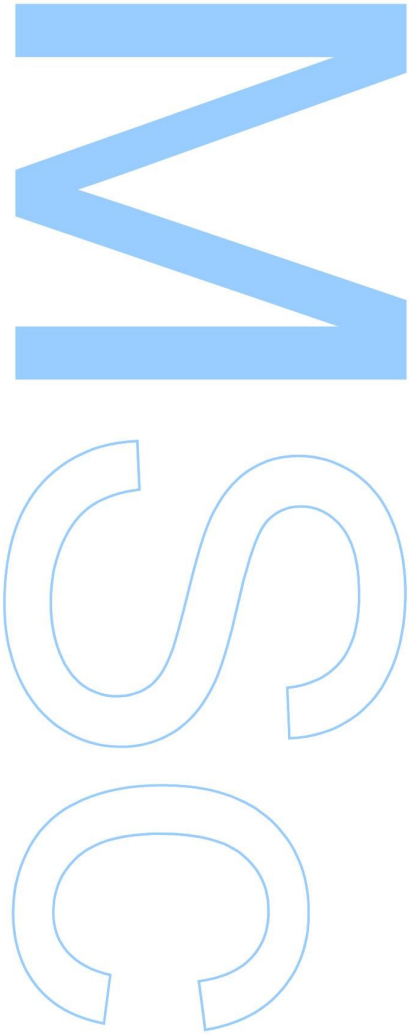

Todas as correções determinadas pelo júri, e só essas, foram efetuadas.

O Presidente do Júri,

Porto, / /

Acknowledgments

First of all, my sincerest thanks to my supervisors, Dr. João Lopes and Dr. João Penedones, for all their availability during the work, for all their patience and for teaching me to have more physical insight of the mathematical equations.

All this work would not be possible without teachers that prepared me very well for future problems. I would like to thank my teachers of Licenciatura and of Mestrado. It was an honor learning with you.

Academic life is not confined to studies; it also includes the friendships that we made, the friends that help us, that make us laugh and that we know we will always can count on them. Therefore, I would like to thank Daniel Passos, Ester Simões, José Pedro Vieira, Pedro Rodrigues and Tiago Magalhães.

A very special word of gratitude to my parents, Quintino Cosme and Luísa Silva, and to my sister, Inês Cosme, for supporting my choices, for their care and love. You are my safe haven.

Finally, I would like to thank Vasco Gonçalves. It was he who helped me most, who supported me most, who put up with me most, during these years. I thank him for helping me to grow up as a person, for hearing my grumbling when I was not satisfied with my work, for being patient and for never giving up on me. Thank you for reminding me every day that life is hard, it has many obstacles; however, if we fight harder, we can overcome them. After all, what really matters is not giving up of our dreams.

Resumo

Os fenómenos críticos são ubíquos em Física e a sua gama de aplicabilidade vai desde Física Estística até à Física de Partículas. Neste contexo, o modelo de Ising crítico é um exemplo paradigmático.

Esta tese foca-se principalmente no estudo dos pontos críticos para o modelo de Ising em duas e em três dimensões, usando métodos de Monte Carlo.

Por fim, nós testamos as previsões de invariância conforme para funções de um e dois pontos do modelo de Ising a três dimensões, com uma superfície esférica.

Abstract

Critical phenomena is ubiquitous in physics and its applicability ranges from statistical to particle physics. In this context, the critical Ising model is a paradigmatic example.This thesis is mainly focused in the study of the critical point for the Ising model in two and three dimensions using Monte Carlo methods.

Finally, we test the predictions of conformal invariance for one and two point functions of the three dimensional Ising model with a spherical boundary.

Contents

List of Tables

List of Figures

Chapter 1

Introduction

The goal of this chapter is to review the main concepts of critical phenomena in statistical systems and of conformal field theory.

1.1 Phase transitions

Phase transitions are abrupt changes of physical observables, when the external fields, e. g., temperature or pressure, are smoothly varied. The special values at which these changes occur are called critical points. In the specific case of the temperature, we shall denote its critical value by T_c . In phase transitions, there is a quantity that is zero in one of the sides of the transition, and it is different from zero in the other side: it is the order parameter. The order parameter distinguishes the different phases of the system and it is associated to a spontaneous symmetry breaking. The behavior of the local fluctuations of the order parameter give us a way to characterize the nature of the transition.

There are two types of phase transitions. In first order (or discontinuous) phase transitions, as is the case of liquid-gas transition in water, the order parameter is the density and it suffers a jump at the critical point. In this case, a first derivative of the free energy of the system is discontinuous.

The other kind of phase transitions is the second order (or continuous) phase transition, e.g. 2D or 3D Ising ferromagnet and critical opalescence in water. The Ising ferromagnet models the interaction of spins assuming each degree of freedom (i.e., the spin) interacts just with the nearest neighbor and it has two possible states: the spin can be either up or down. The order parameter in this example is the absolute value of the magnetization of the system. In this case, when $T < T_c$, the limits $H \to 0^+$ and $H \to 0^-$ (H denotes magnetic field) provide different values for the magnetization. This is an example of the spontaneous symmetry breaking that we referred above: in spite of the Hamiltonian being invariant under simultaneous reversal of all magnetic degrees of freedom, this symmetry is not respected by the thermodynamic equilibrium state. At high temperatures the thermal fluctuations should dominate and

so, the order parameter should be zero in the thermodynamic limit. As the temperature is decreased, the interactions of the system begin to be more important and at the critical temperature the absolute magnetization starts to be non-zero. In this case, the order parameter varies continuously at the critical point, as we can see in fig. (1.1). The relation between the magnetization and the temperature, for 2D Ising model, near the critical temperature, is given by $|m| \sim (T - T_c)^{\frac{1}{8}}$, as we will see in sections below. This type of scaling between two measurable quantities is universal to several systems, even if the microscopic description of each of the systems differ (we will refer an explanation for this phenomenon when we discuss the renormalization group, in section 1.5). At the critical point, there are correlations of all distances between the degrees of freedom and the correlation length [1] becomes infinite. Thus, the strong correlations between a large number of degrees of freedom makes the study of second order phase transitions more complicated, in general. However, there are techniques developed to study critical phenomena. One of them is the renormalization group.

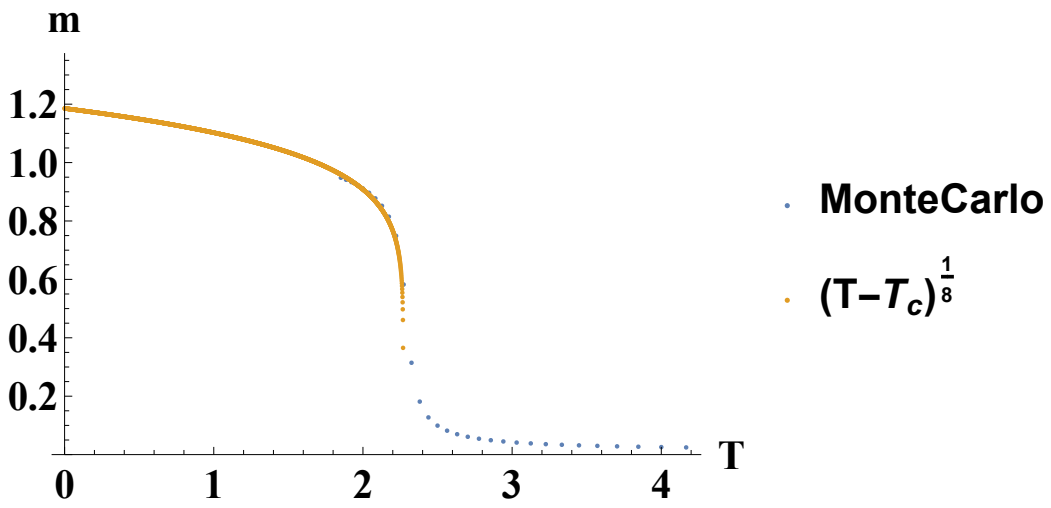

Figure 1.1: The blue dots were obtained using Monte Carlo simulations of a 2D Ising system for a finite lattice 64^2 of size. The orange dots represent the theoretical result for the magnetization for the 2D Ising model $|m| \sim (T_c - T)^{\frac{1}{8}}$.

1.2 Correlation length and correlation function

One of the most important quantities that features a system is the correlation length. The correlation length, usually represented by ξ, is the distance over which the fluctuations of microscopic degrees of freedom - such as the directions of spins, for example - in one region of space are influenced (or

[1] The correlation length ξ measures the range of the correlation function. A more detailed explanation about correlation length and correlation function will be given in the next sections.

correlated with) by fluctuations in another region. If the distance between two spins is larger than this length, we can say that they are practically uncorrelated, because their fluctuations will not affect each other significantly.

In first order phase transitions, the correlation length is finite at the transition temperature, while in second order phase transitions, the correlation length becomes infinite, i.e., diverges, which means that points far apart become correlated.

An important observable in critical phenomena is the correlation function. This function measures how the microscopic variables at different positions are correlated. In other words, it measures the order of the system. The correlation function is positive if the values of those variables fluctuate in the same direction, and it is negative if they fluctuate in opposite directions. It takes zero value if the fluctuations are uncorrelated. The connected correlation function of n-points, $G_c^{(n)}(i_1, i_2, i_3..., i_n)$, is defined by:

$$G_c^{(n)}(i_1, i_2, i_3, ..., i_N) \equiv G^{(n)} - \sum_{partitions} product\, of\, G_c^{(m)},\, with\, m < n \tag{1.1}$$

where i_N is the position of a local observable of the system and $G^{(n)}$ is the whole n-point correlation function. One example is the two-point correlation function between spins at sites i and j:

$$G^{(2)}(i, j) = \langle (s_i - \langle s_i \rangle)(s_j - \langle s_j \rangle) \rangle . \tag{1.2}$$

If the system is translationally invariant, the correlation function only depends on the difference between positions i and j. Moreover, if the system is also isotropic, the function only depends on the distance between spins i and j, $|i - j|$. In the theory of critical phenomena, one is often interested in isotropic lattices and, therefore, it is usual consider $G^{(2)}$ only function of $|i - j|$. Thereby, (1.2) can be rewritten as:

$$G^{(2)}(r) \equiv \langle s_i s_j \rangle - \langle s_i \rangle^2, \tag{1.3}$$

where $r \equiv |i - j|$.

The correlation function should also depend on the correlation length since it measures how the degrees of freedom are separated. Generically, the two point function decays exponentially over large distances.

In second order phase transitions, if the system is not at T_c, the spins become uncorrelated as r increases and the correlation function decays to zero exponentially:

$$G^{(2)}(r) \sim r^{-\tau} e^{-r/\xi}, \tag{1.4}$$

where τ is some number and ξ is the correlation length.

At the critical point, the correlation length becomes infinite and eq. (1.4) does not work. From

experiments and exactly soluble models, the correlation function decays as power law:

$$G^{(2)}(r) \sim \frac{1}{r^{d-2+\eta}}, \tag{1.5}$$

where d is the dimensionality of the system and η is a critical exponent. We will define and explore the critical exponents in section 1.4.

1.3 Brief summary of Ising Model

The goal of the Ising model is to describe the simplest possible interaction between a system of spins. For the one dimensional case the Ising model is exactly solvable, even in the presence of a magnetic field. However, it does not possess a phase transition at finite temperature. So, it is not the most interesting case for studying critical phenomena. In higher dimensions, the Ising model has a phase transition, but solving the problem becomes harder. The 2D Ising Model without magnetic field has an analytical solution, which was achieved by Lars Onsager in 1944 [2], however, the analytical solution for the case $H \neq 0$ has not been discovered yet. For higher dimensions, there is no analytical solution and in the particular case of the Ising in three dimensions we usually resort to numerical studies[2] to access the physical quantities.

The Ising model works in this way: we have a set of spins that interact with first neighbors. This system can be in a magnetic field. To simplify, we will consider, in this study, that there is no magnetic field. In this case, the Hamiltonian is:

$$\mathcal{H} = J \sum_{\langle ij \rangle}^{N} (1 - \sigma_i \sigma_j), \tag{1.6}$$

in which $\langle ij \rangle$ stands for nearest neighbors, σ_i is the spin at position i and can take two possible values: $+1$ or -1 (representing the spin "up" or "down") and J is the constant interaction between spins (we suppose that it does not depend on site; however, in most general cases, it can depend, and we have a constant $J_{i,j}$ for each pair $\sigma_i \sigma_j$).

The order parameter is the absolute magnetization of the system per spin (see section 1.1 for the meaning of order parameter):

$$|m| = \frac{1}{N} \left| \sum_i \sigma_i \right|, \tag{1.7}$$

where N is the total number of spins. This sum is over all points of the lattice.

[2] Even if the Ising model for three dimensions is not known it is still possible to extract information analytically using approximations. In this context we mention the ϵ and the high temperature expansions.

For $T > T_c$, the system is in paramagnetic phase (disordered spins, more symmetric phase) and for $T < T_c$, the system is in ferromagnetic phase (ordered spins, less symmetric phase). When $T = T_c$, regions that are ferromagnetic and other that are paramagnetic coexist together. Here, the correlation length is infinite; if we have a finite sample, it will be restricted by the linear length of the system, L. Thus, for a finite system, there is no phase transition. In fact, it is easy to understand: phase transitions are characterized by divergence when the temperature is varied smoothly. However, all thermodynamic quantities can be obtained from the partition function that, naively, is a completely regular function of the temperature T. Remember that the partition function is given by a sum over all states of the factor $e^{-\beta E}$ (β is $\frac{1}{k_B T}$, where k_B is the Boltzmann constant, and E is the energy of the system) and it is only because there is an infinite number of terms that the sum can get a divergence as a function of T. In the one dimensional Ising model, there is no phase transition at finite temperature. The critical temperature for the 2D Ising model is

$$T_c = \frac{2J}{\ln\left(1+\sqrt{2}\right)}. \tag{1.8}$$

The main goal of this work is to study the critical point of the three dimensional Ising model using Monte Carlo methods. We will use $J = 1$ and set $k_B = 1$. In this numerical approach, we will not be able to simulate an infinite system, so we know before hand that there is no critical point in the particular case we are dealing. However, it is possible to extract the information of the observables of the critical Ising model by analyzing how the finite system scales with size; this is called finite size scaling. We will discuss it in chapter 4.

1.4 Critical Exponents and Universality

As described before, the two point function in a critical system decays as a power law. The exponent of the power is one example of critical exponent. More concretely, they describe the behavior of physical observables, such as specific heat or magnetic susceptibility, when the external fields are varied near the critical point. Let us consider a function f that depends on t. Then, the critical exponent is defined by:

$$\lambda = \lim_{t\to 0} \frac{\ln|f(t)|}{\ln|t|}, \tag{1.9}$$

where t is the reduced temperature, defined by:

$$t = \frac{T - T_c}{T_c}. \tag{1.10}$$

Magnetization ($H = 0$)	$m \sim (-t)^{\beta}$
Specific Heat ($H = 0$)	$C_H \sim \|t\|^{-\alpha}$
Isothermical Susceptibility ($H = 0$)	$\chi_T \sim \|t\|^{-\gamma}$
Critical Isotherm ($t = 0$)	$m \sim h^{\frac{1}{\delta}}$
Correlation Length	$\xi \sim \|t\|^{-\nu}$
Spin-spin Correlation Function	$G(r) \sim \frac{1}{r^{d-2-\eta}}$

Table 1.1: Definitions of the most used critical exponents for magnetic systems. h stands for magnetic field divided by $k_B T$. Table from ref. [23].

For example, $f(t)$ can be the magnetization per spin as function of the reduced temperature t. Thereby, the thermodynamic function, depending on t, can be written as sum of powers:

$$f(t) = A|t|^{\lambda}\left(1 + Bt^{\gamma} + ...\right). \tag{1.11}$$

Near the critical point, the function behaves like:

$$f(t) \sim |t|^{\lambda}, \tag{1.12}$$

The critical exponents are important because they can be measured, and so, give us some clues about the thermodynamic features of the system we are studying. We can think that using the whole function is better and we can collect more information; however, in most of the systems, we can not have access to the whole thermodynamic function.

One of the advantages of knowing the critical exponents is that they are **universal.** We say that a quantity is universal when its properties depend on general features (namely, the dimensionality of space, the dimension of order parameter, symmetries), but do not depend on microscopic details of interactions.

We can match a system to a universality class. The systems that belong to the same universality class have the same critical exponents. This is very important because when we are studying the properties of one system, we can relate it with properties of another system that has the same critical exponents. For example, the endpoint of the liquid-gas phase transition of water and the phase transition that occurs in a Ising ferromagnet exhibit the same characteristics, although they are very different systems. So, when we study the 3D Ising Model, we are learning about the phase transition of water too.

To conclude this section, the table (1.1) contains the definitions of the most used critical exponents for magnetic systems.

1.5 Renormalization Group Transformation

One is often interested in observables which vary smoothly or, in other words, in the long wave length. In this context, it is not hard to believe that fine details of the microscopic interaction do not alter significantly long range effects. The renormalization group tries to study how a given model, i.e., the Hamiltonian or Lagrangian, gives rise to large distance physics. The philosophy of the method is simple. Let us consider a system with many degrees of freedom distributed over space. Now, we just try to integrate the degrees of freedom which are a given distance apart. In the case that the renormalization group is done in real space and in a spin lattice system, we can view this as summing over a given set of spins and rescale the lattice size at the end. This rescaling is important, as we will be trying to compare the original and transformed interactions. This is a process that can be done repeatedly, generating a flow in the space of all possible Hamiltonians or Lagrangians. The endpoint of this flow is called the fixed point. Let us remark that it is possible that two nearby Hamiltonians in this space of all possible interactions will land on the same fixed point. This is nothing more than what was called universality. Implementations of the renormalization group often involve approximations that if well made do not affect the end results. Let us be more concrete and consider an Hamiltonian $\mathcal{H}$, and denote the action of the renormalization group as

$$\mathcal{H}' = \mathcal{R}\mathcal{H}, \tag{1.13}$$

in which $\mathcal{H}'$ is the renormalized Hamiltonian of the new system and $\mathcal{R}$ is the renormalization group operator. This operation decreases the number of degrees of freedom from N to N'. The renormalization transformation can be done in real space, by removing or grouping spins, or in momentum space, by integrating out large wavevectors. The scale factor of the transformation, b, is defined by:

$$b^d = \frac{N}{N'}, \tag{1.14}$$

where d is the dimensionality of the space. In the following we will present a detailed analysis of the action of the renormalization group in the space of all possible interactions. We will conclude that some interactions are relevant, i.e., they determine which fixed point the system will approach, and other are irrelevant. In the next subsection we show a general example of the renormalization group to make the transition to the theory more smooth.

1.5.1 The Block Spin Transformation

In this section we will present an example of a particular renormalization group scheme, called block spin transformation. For concreteness, consider a spin system over a d- dimensional lattice with spacing

a. The whole purpose of RG is to integrate over short degrees of freedom, in this case, divide the lattice in blocks, say of size $l \times l \cdots \times l$, containing l^d spins, and sum over all the spins in each block except one. Then we would be left with an effective interaction for the representative spin of the renormalized block. One such scheme is the block spin transformation where for the representative of the spin of a block we take the majority rule. For this purpose, one defines the function:

$$T\left(s';s_1,...,s_{l^d}\right)=\begin{cases}1, & s'\sum_i s_i>0;\\ 0 & otherwise\end{cases}. \tag{1.15}$$

The Hamiltonian describing the interactions of new spin is defined by:

$$\exp\left(-\mathcal{H}'\left(s'\right)\right)\equiv Tr_s\prod_{blocks}T\left(s';s_i\right)\exp\left(-\mathcal{H}\left(s\right)\right), \tag{1.16}$$

Consider that we have a lattice of spins, whose partition function is:

$$Z=Tr_s\exp(-\mathcal{H}(s)), \tag{1.17}$$

(the β constant was absorbed into the definitions of the parameters of $\mathcal{H}$). Notice that the partition function computed with the new Hamiltonian or with the old one are the same:

$$\mathrm{Tr}_{s'}e^{-\mathcal{H}'(s')}=\mathrm{Tr}_s e^{-\mathcal{H}(s)}, \tag{1.18}$$

where we have used $\sum_{s'}T\left(s';s_i\right)=1$. Moreover, the new Hamiltonian preserves not just the partition function but also all the physics whose wave length is considerably larger than the typical size of the block. This will be important to study how correlation functions transform under RG action. However, this method is not practical in most cases and more approximations must be done to carry on the computation.

1.6 Scaling variables, Scaling Function and Critical Exponents

The goal of this section is to explain the theory behind the renormalization group (RG), applying the ideas present in the last subsection to the space of all couplings. In the following we shall denote by $\{K\}$ this space, then the action of the renormalization group relates the couplings of the transformed system $\mathcal{R}H$ to the original one,

$$\{K'\}=\mathcal{R}(\{K\}), \tag{1.19}$$

where $\mathcal{R}$ depends on the specific transformation chosen and on the parameter b. This equation tells us that the couplings of the new system are obtained by combinations of the original. Again, this is a process that can be done iteratively and will generate a path in the space of all possible couplings. The fixed point in this path is defined by the condition

$$\{K^*\} = \mathcal{R}\{K^*\}. \tag{1.20}$$

The operation $\mathcal{R}$ depends on the scale b and in principle we can set this scale to be arbitrarily close to 1, $b = 1 + \delta$. Close to a fixed point we can write the following system of equations:

$$K'_a - K^*_a \simeq \sum_b T_{ab} \left(K_b - K^*_b\right), \tag{1.21}$$

where we used $T_{ab} = \frac{\partial K'_a}{\partial K_b} \mid_{K=K^*}$. This matrix tells how is the behavior of the renormalization group near the fixed point. By definition, T_{ab} does not have to be symmetric and in general it is not. Let us represent the eigenvalues of T by λ^i and the left eigenvectors as $\{e^i\}$[3],

$$\sum_a e^i_a T_{ab} = \lambda^i e^i_b. \tag{1.22}$$

There is a specific linear combination of $K_a - K^*_a$ such that it is an eigenvector of the renormalization group, to this specific linear combination of variables we call **scaling variables.** More rigorously, they are defined in the following way:

$$u_i = \sum_a e^i_a \left(K_a - K^*_a\right). \tag{1.23}$$

From (1.21), (1.22) and (1.23) we can easily check that, near the fixed point, scaling variables transform multiplicatively or, in other words, they are eigenvectors of the RG action:

$$\begin{aligned} u'_i &= \sum_a e^i_a (K'_a - K^*_a) \\ &= \lambda_i u_i. \end{aligned} \tag{1.24}$$

The renormalization group action depends on the scale factor b and so the eigenvalues must also have this dependence. Since the correlations in critical systems are characterized by power laws it is convenient to write the eigenvalues λ_i as

$$\lambda_i = b^{y_i}, \tag{1.25}$$

where the variable y_i is related with the critical exponents, as we will see soon.

[3]Remember that in the case where the a matrix is not symmetric the right and left eigenvectors do not need to be the same.

When $y_i > 0$, u_i is relevant; it means that applying renormalization group transformations several times will move u_i away from the fixed point. If $y_i < 0$, u_i is irrelevant, that is, applying renormalization group transformations several times will approximate u_i to the fixed point. Finally, if $y_i = 0$, u_i is marginal, i.e., we do not know, by linearized equations (1.21), if u_i is moving away from the fixed point or towards it.

The Ising Model has two relevant scaling variables: a thermal scaling variable, u_t, with eigenvalue y_t and a magnetic scaling variable, u_h, whose eigenvalue is y_h. Near the critical point, u_t and u_h are proportional to t (temperature) and h (magnetic field), respectively. When $t = 0$ and $h = 0$, u_t and u_h vanish. So, we have the following relations:

$$u_t = \frac{t}{t_0} + O\left(t^2, h^2\right) \tag{1.26}$$

$$u_h = \frac{h}{h_0} + O\left(th, h^3\right), \tag{1.27}$$

in which t_0 and h_0 are constants (non-universal).

It is possible to get the free energy per spin, as function of the couplings $\{K\}$:

$$f\left(\{K\}\right) = -\frac{1}{N}\ln\left(Z\right). \tag{1.28}$$

Under renormalization, and if $\{K\}$ does not include a constant in Hamiltonian, the free energy $f\left(\{K\}\right)$ transforms inhomogeneously:

$$f\left(\{K\}\right) = g\left(\{K\}\right) + b^{-d} f\left(\left\{K'\right\}\right). \tag{1.29}$$

This is the fundamental transformation equation for the free energy. It is easy to verify that free energy transforms inhomogeneously when one applies renormalization. Nevertheless, for obtaining the critical exponents, we are only interested in the singular part of the free energy, that is constituted merely by f. We can neglect the term $g\left(\{K\}\right)$, assuming that it comes from summing over the short wavelength degrees of freedom. For that reason, g is an analytic function of K everywhere.

Therefore, the transformation law for the singular part of the free energy is:

$$f_s\left(\{K\}\right) = b^{-d} f_s\left(\left\{K'\right\}\right). \tag{1.30}$$

Near the fixed point, we can write (1.30) as function of the scaling variables:

$$f_s(u_t, u_h) = b^{-d} f_s(b^{y_t} u_t, b^{y_h} u_h). \tag{1.31}$$

And if we iterate the renormalization group n times, we get:

$$f_s\left(u_t, u_h\right) \quad = \quad b^{-nd} f_s\left(b^{ny_t} u_t, b^{ny_h} u_h\right). \tag{1.32}$$

We have to be careful with the number of iterations, once that u_t and u_h increase as we increase the number of iterations. If n is too big, the linear approximation to the renormalization group equations can not be valid. To control this problem, we stop the iteration when we get the condition:

$$|b^{ny_t} u_t| = u_{t_0}, \tag{1.33}$$

in which u_{t_0} is arbitrary and it is small enough to allow the approximation. Thus,

$$f_s\left(u_t, u_h\right) = \left|\frac{u_t}{u_{t_0}}\right|^{\frac{d}{y_t}} f_s\left(\pm u_{t_0}, u_h \left|\frac{u_t}{u_{t_0}}\right|^{-\frac{y_h}{y_t}}\right). \tag{1.34}$$

Rewriting the last expression, using (1.26) and (1.27), we see that u_{t_0} can be embedded into a redefinition of the scale factor t_0, and so

$$f_s\left(t, h\right) = \left|\frac{t}{t_0}\right|^{\frac{d}{y_t}} \Phi\left(\frac{h/h_0}{|t/t_0|^{\frac{y_h}{y_t}}}\right). \tag{1.35}$$

Φ is the **scaling function** and it is universal. From it, we can relate all the critical exponents of table (1.1) with the eigenvalues of the scaling variables:

- Spontaneous magnetization, m:

$$\begin{aligned} m &= \frac{\partial f}{\partial h}|_{h=0} \\ &\propto (-t)^{(d-y_h)/y_t} \end{aligned} \tag{1.36}$$

$$\Rightarrow \quad \beta = \frac{d - y_h}{y_t} \tag{1.37}$$

- Specific heat, C_H:

$$\begin{aligned} C_H &= \frac{\partial^2 f}{\partial t^2}|_{h=0} \\ &\propto |t|^{\frac{d}{y_t}-2} \end{aligned} \tag{1.38}$$

$$\Rightarrow \quad \alpha = \quad 2 - \frac{d}{y_t} \tag{1.39}$$

- Magnetic susceptibility, χ_H:

$$\begin{aligned} \chi_H &= \frac{\partial^2 f}{\partial h^2}|_{h=0} \\ &\propto |t|^{\frac{(d-2y_h)}{y_t}} \end{aligned} \tag{1.40}$$

$$\Rightarrow \quad \gamma = \quad -\frac{(d-2y_h)}{y_t} \tag{1.41}$$

- Magnetization with $H \neq 0$:

$$\begin{aligned} m &= \frac{\partial f}{\partial h} \\ &= \left|\frac{t}{t_0}\right|^{\frac{d-y_h}{y_t}} \Phi'\left(\frac{h/h_0}{\left|\frac{t}{t_0}\right|^{\frac{y_h}{y_t}}}\right) \end{aligned} \tag{1.42}$$

In this case, in order to m have a finite limit as $t \to 0$, the function $\Phi'(x)$ must behave like a power of x as $x \to \infty$. Let us say that when $x \to \infty$, $\Phi'(x) \to x^a$. Now, we can substitute this expression in (1.42), and we verify that $a = \frac{d-y_h}{y_h}$ so that m be finite when $t \to 0$. Therefore, we obtain:

$$m \quad \propto \quad h^{\frac{d-y_h}{y_h}} \tag{1.43}$$

$$\Rightarrow \delta = \frac{y_h}{(d-y_h)}. \tag{1.44}$$

1.7 Correlation function of scaling operators

The action of the renormalization group maps one set of couplings from a given Hamiltonian to a new set of couplings. This is done by integrating some of the degrees of freedom, so computing the partition function using the original or renormalized Hamiltonian should give the same result,

$$Z = \sum_{\{s_i\}} e^{-\beta\mathcal{H}} = \sum_{\{s_i'\}} e^{-\beta\mathcal{H}'}. \tag{1.45}$$

However, the renormalization group action preserves more than the partition function, when we are interested in the long wave length physics. The goal of this subsection is to study how RG constrains the form of correlation function of two variables. Consider the two point function of two spins localized at r_1 and r_2 in the Ising model,

$$G\left(r_1 - r_2, \mathcal{H}\right) = \frac{\partial^2 \ln Z}{\partial h\left(r_1\right) \partial h\left(r_2\right)}, \tag{1.46}$$

in which we have introduced a non-uniform magnetic field, which can be switched off at the end of the computation, if necessary, and we have made explicit the dependence on the Hamiltonian $\mathcal{H}$. Under RG the interactions become different, more concretely,

$$\mathcal{H} - \sum_r s\left(r\right) h\left(r\right) \rightarrow \mathcal{H}' - \sum_{r'} s'\left(r'\right) h'\left(r'\right). \tag{1.47}$$

We can compute the same correlation function but now, using the renormalized action,

$$G\left(\frac{r_1 - r_2}{b}, \mathcal{H}'\right) = \frac{\partial^2 \ln Z}{\partial h'\left(r_1'\right) \partial h'\left(r_2'\right)}, \tag{1.48}$$

where we have used that the partition function is invariant under RG. Beyond that, in lattice spacing units, the distance between the points was decreased by a factor of b. We are interested in the case of short range interactions, in which we can assume that the magnetic field transforms uniformly under RG, i.e. $h'\left(r'\right) = b^{y_h} h\left(r\right)$. The left hand-side of (1.48) is the correlation function of the block, when we have the renormalized Hamiltonian. The right-hand side of the equation is more subtle. We can perform the following local infinitesimal change in block of spins 1:

$$h'\left(r_1'\right) \longrightarrow h'\left(r1'\right) + \delta h'\left(r_1'\right). \tag{1.49}$$

This corresponds to a change of all fields $h\left(r_i\right)$, that act in the spins of this block, by an amount $\delta\left(r_i\right) = b^{-y_h} \delta h'\left(r_1'\right)$. In this way, we get, for the right-hand side of (1.48),

$$b^{-2y_h} \left\langle \left(s_1^{(1)} + s_2^{(1)} + ...\right) \left(s_1^{(2)} + s_2^{(2)} + ...\right) \right\rangle_{\mathcal{H}}, \tag{1.50}$$

where the spins of the blocks 1 and 2 are labeled by $s_i^{(1)}$ and $s_i^{(2)}$ and the subscript $\mathcal{H}$ indicates that the correlation function is evaluated with respect to the original Hamiltonian. There are b^d spins in each block, so, we are able to expand (1.50) as a sum of b^{2d} two point correlations. If $|r_1 - r_2| >> b$, all correlation functions are, numerically, almost the same. Using this, we arrive at the following equality

relating the original and transformed correlation function:

$$G\left(\frac{r_1 - r_2}{b}, \mathcal{H}'\right) = b^{2(d-y_h)} G\left(r_1 - r_2, \mathcal{H}\right), \tag{1.51}$$

Now, we can simply set the magnetic field to zero and we get:

$$G\left(r, t\right) = b^{-2(d-y_h)} G\left(\frac{r}{b}, b^{y_t} t\right), \tag{1.52}$$

where we have assumed that the system is rotation invariant and, for convenience, setting $|r_1 - r_2| = r$. Such as we did in (1.32), we can iterate (1.52) n times. In this case, we stop the iteration at $b^{n y_t}\left(\frac{t}{t_0}\right) = 1$. Therefore, we get:

$$G(r, t) = \left|\frac{t}{t_0}\right|^{\frac{2(d-y_h)}{y_t}} \Psi\left(\frac{r}{|t/t_0|^{-\frac{1}{y_t}}}\right). \tag{1.53}$$

For large r, as we already referred, $G \sim \exp(\frac{-r}{\xi})$. As stated in Table (1.1), $\xi \sim |t|^{-\nu}$. We can identify $\xi \sim |t|^{\frac{-1}{y_t}}$ in (1.53). Therefore, we obtain the following relation:

$$\nu = \frac{1}{y_t}. \tag{1.54}$$

At the critical point, $t = 0$, this equation tells us that the correlation function should decay as

$$G\left(r, 0\right) \propto r^{-2(d-y_h)}. \tag{1.55}$$

Thus, the decay of this correlation function at criticality is determined by renormalization group eigenvalue y_h.

We will now move to correlation functions of other fields. Recall that the scaling variable u_i can be written in terms of the coupling $K_i - K_i^*$. These interactions are associated with fields S_i in the Hamiltonian. Scaling operators ϕ_i are defined by,

$$\sum_i u_i \phi_i = \sum_a \left(K_a - K_a^*\right) S_a. \tag{1.56}$$

By promoting the variables to have a space position $u_i\left(r\right)$, we can mimic almost exactly the same derivation for correlation functions of two operators ϕ_i:

$$\left\langle \phi_i\left(r_1\right) \phi_j\left(r_2\right) \right\rangle \propto r^{-2(d-y_i)}. \tag{1.57}$$

Let us just emphasize that, given a product of local operators, they will not be, in general, scaling operators and, consequently, their correlation function will not have this simple power law decay.

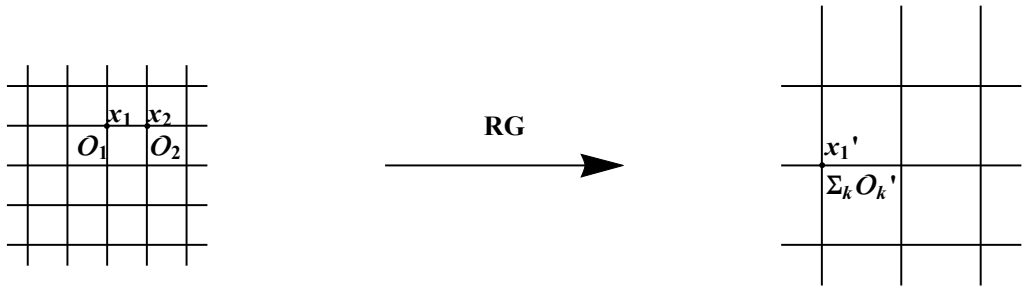

Figure 1.2: The idea behind the OPE is that two operators sitting close together, as in the figure of the left-hand side, are mapped to an effective operator just at one point under RG action, as can be seen on the figure of the right-hand side.

1.7.1 Operator Product Expansion

The goal of this subsection is to introduce the concept of operator product expansion (OPE), that is ubiquitous in statistical physics and quantum field theory. Consider a lattice system with two fields located at points x_1 and x_2. Then, under a typical RG action, these points can be transformed into one, which we denote by x_1'. Thus, in the original system, there were two fields at different points. However, under RG these were mapped to single effective field - fig.(1.2).

In the vicinity of a critical point we can think that these operators are scaling fields, more concretely, we have one operator ϕ_1 at point x_1 and another operator ϕ_2 at point x_2. These operators can be expressed in terms of the product local fields S_a . Under RG action this product will be mapped to a different set of fields, say S_a', but at a single point. Then, we can rewrite these new fields in terms of scaling operators $\sum_k \phi_k$. Thus, we conclude that generically we have

$$\phi_1(x_1)\,\phi_2(x_2) \to \sum_k \phi_k(x_1)\,. \tag{1.58}$$

This is valid as long as there are no other operators in the neighborhood of these two operators and when it is evaluated inside a given correlation function. As we will see in the following section, the OPE is an identity which is extremely important in the context of conformal field theories.

1.8 Conformal and scale invariant field theories

The action of the renormalization group changes the system size, integrating out all degrees of freedom which are shorter than a specified cut-off. The critical point is a fixed point in this action, so the system at this special point is not changed under the RG action. Thus, at the critical point, we are interested in the long wave length interactions, i.e., with continuous description. By definition, the fixed point should have

an additional symmetry, namely it is invariant under scale transformations. Scale invariant theories, sometimes, get their symmetry enlarged to conformal symmetry (translations, dilations, rotations and special conformal transformations, that we will explain in the next subsection). This amounts to having also inversion symmetry. The necessary and sufficient conditions to have this enlargement of symmetry in a field theory are not completely understood yet. In 2D it was proved that this is the case, i.e., once the system is scale invariant and unitary it is also conformal invariant. In higher dimensions, it was recently proved just for $d = 4$ [19].

The 3D Ising model at the critical temperature is obviously scale invariant. One of the main goals of this thesis is to verify if, in the continuum limit, this theory is also conformal invariant. For this purpose, we will look for specific signatures of conformal symmetry that are not implied by scale symmetry. So we will begin by explaining the basic properties of the conformal symmetry and then we will analyze a system with boundary. In the presence of a boundary, there is a substantial difference between conformal and scale symmetry.

1.8.1 Conformal Transformations

A conformal field theory has the following symmetries:

- translations:

$$\left(x'\right)^{\mu} = x^{\mu} + a^{\mu}; \tag{1.59}$$

- dilations:

$$\left(x'\right)^{\mu} = \alpha x^{\mu}; \tag{1.60}$$

- rotations:

$$\left(x'\right)^{\mu} = M^{\mu}_{\nu} x^{\nu} \tag{1.61}$$

- inversions:

$$\left(x'\right)^{\mu} = \frac{x^{\mu}}{x^2} \tag{1.62}$$

- special conformal transformation, SCT, that is a inversion followed by a translation that, in turn, is followed by another inversion:

$$\left(x'\right)^{\mu} = \frac{x^{\mu} - b^{\mu} x^2}{1 - 2b.x + b^2 x^2} \tag{1.63}$$

$$= \frac{\frac{x^{\mu}}{x^2} - b^{\mu}}{\left(\frac{x^{\mu}}{x^2} - b^{\mu}\right)^2} \tag{1.64}$$

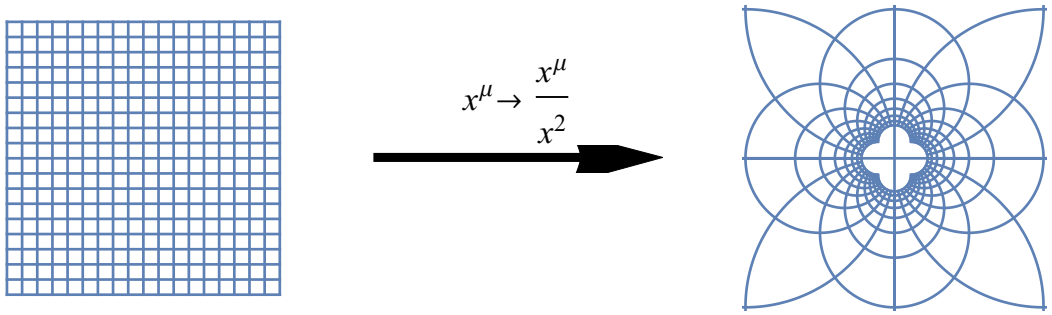

Figure 1.3: On the image of the left-hand side, we plot a series of horizontal and vertical lines that intersect at right angles. After an inversion, around the origin, this image is mapped to the right-hand side plot. Each line on the left-hand side is transformed to a circle. Notice, however, that at the intersection points, the angles remain with $\frac{\pi}{2}$.

The inversion symmetry is not connected to the identity, so it is usual to introduce the connected part of the conformal group by replacing the generator of inversions by special conformal transformations generator, K^μ, defined by,

$$K^\mu = IP^\mu I,$$

where P^μ denotes translations and I an inversion.

The conformal group is associated with the symmetries that preserve angles. It is obvious that translations, rotations and dilations preserve the angle between two intersecting lines. In fig. (1.3) we plot an example of inversion symmetry and we verify that it preserves the angles too.

1.8.2 Correlation functions

Operators belonging to a conformal field theory are of one of two types, they are either primary or they are descendants. The distinction between the two is: a primary operator is killed by the action of the generator of the special conformal transformations, K^μ

$$\hat{K}_\mu \left|\mathcal{O}\right\rangle = 0, \tag{1.65}$$

where $\left|\mathcal{O}\right\rangle \equiv \hat{\mathcal{O}}\left(0\right)\left|0\right\rangle$; in turn, the descendants operators are obtained from the primary operator just by acting with the generator of translations, P^μ:

$$i\hat{P}_\mu \left|\mathcal{O}\right\rangle = \partial_\mu \hat{\mathcal{O}}\left(0\right)\left|0\right\rangle, \tag{1.66}$$

in which $\partial_\mu \hat{\mathcal{O}}(0)$ is the descendant operator. Each operator carries with it two quantum numbers, the dimension and the spin, which are associated with the generator of scale transformation and rotations respectively. In conformal field theories, we are usually interested in studying correlation function of local operators,

$$\langle \mathcal{O}_1(x_1) \dots \mathcal{O}_n(x_n) \rangle = \frac{1}{Z} \int [D\Phi]\, e^{-S} \mathcal{O}_1(x_1) \dots \mathcal{O}_n(x_n), \tag{1.67}$$

where $\int [D\Phi]$ denotes the path integral over all possible configurations of the elementary fields, $\mathcal{S}$ denotes the Euclidean action of the system and Z is the partition function. The correlation function of primary local operators in conformal field theory satisfies the following rule, under conformal transformations:

$$\langle \mathcal{O}_1(x_1) \dots \mathcal{O}_n(x_n) \rangle = \left| \frac{\partial x'^\nu}{\partial x^\mu} \right|^{\frac{\Delta_1}{d}} \dots \left| \frac{\partial x'^\nu}{\partial x^\mu} \right|^{\Delta_n} \langle \mathcal{O}_1(x'_1) \dots \mathcal{O}_n(x'_n) \rangle, \tag{1.68}$$

where $\left|\frac{\partial x'^\nu}{\partial x^\mu}\right|$ is the Jacobian of the transformation and Δ_i is the scaling dimension of $\mathcal{O}_i$. The conformal symmetry is powerful enough to fix completely the position dependence of two and three point functions of local primary operators. For the two point function of scalar primary operators, rotations, translations and dilation imply that

$$\langle \mathcal{O}_1(x_1) \mathcal{O}_2(x_2) \rangle = \frac{1}{(x_{12}^2)^{\frac{\Delta_1+\Delta_2}{2}}}, \tag{1.69}$$

where x_{12} is the distance between the operators $\mathcal{O}_1(x_1)$ and $\mathcal{O}_2(x_2)$. We can write (1.69) as:

$$\langle \mathcal{O}_{\Delta_1}(x_1) \mathcal{O}_{\Delta_2}(x_2) \rangle = f(x_{12}^2). \tag{1.70}$$

Let us suppose that $f(x)$ has the following expansion:

$$\langle \mathcal{O}_{\Delta_1}(x_1) \mathcal{O}_{\Delta_2}(x_2) \rangle = \sum_a \frac{c_a}{(x_{12}^2)^a}. \tag{1.71}$$

Applying scale invariance $x'^\mu = \lambda x^\mu$:

$$\begin{aligned} \langle \mathcal{O}_{\Delta_1}(x_1) \mathcal{O}_{\Delta_2}(x_2) \rangle &= \left|\frac{\partial x'_1}{\partial x_1}\right|^{\frac{\Delta_1}{d}} \left|\frac{\partial x'_2}{\partial x_2}\right|^{\frac{\Delta_2}{d}} \langle \mathcal{O}_{\Delta_1}(x'_1) \mathcal{O}_{\Delta_2}(x'_2) \rangle \sum_a \frac{c_a}{(x_{12}^2)^a} \\ &= \lambda^{\Delta_1+\Delta_2-2a} \sum_b \frac{c_b}{(x_{12}^2)^b} \\ \implies \quad a &= \frac{\Delta_1+\Delta_2}{2}. \end{aligned} \tag{1.72}$$

Notice that, under inversions, we have

$$x'^2_{12} = \frac{x^2_{12}}{x^2_1 x^2_2}, \quad |\frac{\partial x'}{\partial x}| = \frac{1}{(x^2)^d}. \tag{1.73}$$

Therefore, we have:

$$\begin{aligned} \langle \mathcal{O}_{\Delta_1}(x_1)\mathcal{O}_{\Delta_2}(x_2)\rangle &= \frac{1}{(x^2_{12})^{\frac{\Delta_1+\Delta_2}{2}}} \\ &= |\frac{\partial x'_1}{\partial x_1}|^{\frac{\Delta_1}{d}} |\frac{\partial x'_2}{\partial x_2}|^{\frac{\Delta_2}{d}} \langle \mathcal{O}_{\Delta_1}(x'_1)\mathcal{O}_{\Delta_2}(x'_2)\rangle \\ \Rightarrow \quad \frac{1}{(x^2_{12})^{\frac{\Delta_1+\Delta_2}{2}}} &= |\frac{\partial x'_1}{\partial x_1}|^{\frac{\Delta_1}{d}} |\frac{\partial x'_2}{\partial x_2}|^{\frac{\Delta_2}{d}} \frac{(x^2_1 x^2_2)^{\frac{\Delta_1+\Delta_2}{2}}}{(x^2_{12})^{\frac{\Delta_1+\Delta_2}{2}}} \\ &= \frac{1}{(x^2_1)^{\Delta_1}(x^2_2)^{\Delta_2}} \frac{(x^2_1 x^2_2)^{\frac{\Delta_1+\Delta_2}{2}}}{(x^2_{12})^{\frac{\Delta_1+\Delta_2}{2}}} \end{aligned} \tag{1.74}$$

which implies that the two point function is non-zero only if $\Delta_1 = \Delta_2$. For the three point function of scalar primary operators, we have

$$\langle \mathcal{O}_1(x_1)\mathcal{O}_2(x_2)\mathcal{O}_3(x_3)\rangle = \frac{C_{123}}{\left(x^2_{12}\right)^{\frac{\Delta_1+\Delta_2-\Delta_3}{2}} \left(x^2_{13}\right)^{\frac{\Delta_1+\Delta_3-\Delta_2}{2}} \left(x^2_{23}\right)^{\frac{\Delta_2+\Delta_3-\Delta_1}{2}}}. \tag{1.75}$$

Notice that we are always free to choose a normalization such that the two point function is normalized to one. However, if this is done, the coefficient appearing in the three point function is uniquely fixed. An important property of conformal field theories is the OPE expansion,

$$\mathcal{O}_2(x_2)\mathcal{O}_1(x_1) = \sum_k C_{12k} B(x_{12}, \partial_{x_1}) \mathcal{O}_k(x_1), \tag{1.76}$$

where the product of two operators at different points can be replaced by a sum over operators located at a single point. The function $B(y,z)$ can be determined by requiring consistency of the OPE and the explicit result for two and three point functions. This is an operator identity that can be successively used in correlation functions, turning an n-point function into a sum of $(n-1)$-point functions. From what has been said above, we conclude that all information in a conformal field theory is encoded in two and three point functions. In the present work we will be interested mostly in correlation functions of scalar primary operators.

1.8.3 Weyl invariance

A theory is said to have Weyl symmetry if it stays invariant under a Weyl transformation:

$$g_{ab}(x) = \lambda(x)\, g'_{ab}(x), \tag{1.77}$$

where g_{ab} and g'_{ab} are metrics. Notice that this type of transformation leaves the angles between two intersecting lines unchanged. Let us denote by $\langle \dots \rangle_g$ the correlation function of a theory having the metric g. Then, the correlation functions of operators that are related through a Weyl transformation satisfy

$$\langle \mathcal{O}(x_1) \dots \mathcal{O}(x_n) \rangle_g = \langle \mathcal{O}(x'_1) \dots \mathcal{O}(x'_n) \rangle_{g'} \tag{1.78}$$

$$= \left| \frac{\partial x'}{\partial x} \right|_{x=x_1}^{\frac{\Delta_1}{d}} \dots \left| \frac{\partial x'}{\partial x} \right|_{x=x_n}^{\frac{\Delta_n}{d}} \langle \mathcal{O}(x'_1) \dots \mathcal{O}(x'_n) \rangle_{g'}, \tag{1.79}$$

where x' denotes the coordinates in the system with metric g'_{ab} , $\mathcal{O}$ are primary operators and d is the dimensionality of the system. This is the Weyl invariance. In this way, we can relate correlation functions having metrics which are Weyl related.

1.8.4 Boundary conformal field theory - planar boundary

The presence of a boundary in a conformal field theory breaks the symmetry of the system. Then, it is expected that the system is not so constrained. The simplest boundary that one can engineer in a conformal field theory is a planar boundary. Let us consider a system that exists only for $x_d \geq 0$, with x_d being coordinate in a d dimensional theory. The symmetry is reduced in this case; for example, it is only invariant under rotations that preserve the boundary. In this case, the symmetry does not exclude one point functions. For instance, we have

$$\langle \mathcal{O}(x) \rangle = \frac{a}{(x_d)^{\Delta}}, \tag{1.80}$$

where a is a constant.

Correlation functions involving two operators are not completely determined by symmetry. We can understand this fact easily by noticing that the variable

$$\zeta = \frac{(x-y)^2}{x_d y_d} \tag{1.81}$$

is left invariant under scale transformations. ζ is called cross ratio. So, we conclude that the two point function in the presence of the boundary is given by:

$$\langle \mathcal{O}_1(x)\,\mathcal{O}_2(y)\rangle = \frac{g(\zeta)}{\left((x-y)^2\right)^{\frac{\Delta_1+\Delta_2}{2}}}, \tag{1.82}$$

with g an undetermined function of the conformal cross ratio ζ. However, in the limit in which the points are coming close together, $\zeta \to 0$, we know that the function $g(\zeta)$ should go to 1 if $\mathcal{O}_1 = \mathcal{O}_2$. This makes sense because in this limit the operators do not feel the presence of the boundary.

In the presence of the boundary, we have another type of OPE, namely the bulk-to-boundary OPE. In this case, we can replace an operator, that is a small distance apart from the boundary, by a combination of operators living on the boundary

$$\mathcal{O}_1(x) = \frac{1}{x_d^{\Delta_1-\Delta_k}} \sum_k a_{\Delta_k} D(x_d, \partial_{x_d})\,\hat{\mathcal{O}}_k(\vec{x}), \tag{1.83}$$

where we have used the notation $\vec{x} = (x_1, \ldots, x_{d-1}, 0)$. $\hat{\mathcal{O}}_k(\vec{x})$ are operators living on the boundary with scaling dimension Δ_k, the constants a_{Δ_k} are new physical numbers (introduced by the presence of the boundary) and the function $D(x_d, \partial_{x_d})$ encodes the contribution of the descendants operators. Now, we can try to take the limit in which the points of the two point function (1.82) are approaching the boundary. The leading order contribution will be given by the boundary operators with lowest dimension. Notice that for this derivation we have used that two point function of boundary operators, $\hat{\mathcal{O}}$, is completely determined by conformal symmetry. The reason is simple to understand: since these operators are located at the boundary, it is like they are effectively in a $d-1$ system, with conformal symmetry and no boundary.

1.8.5 Boundary conformal field theory - spherical boundary

In the previous case we analyzed the simplest possible boundary that can exist in a conformal field theory. In this subsection, we will study the case where the boundary is spherical. Recall that a spherical boundary is related to a planar boundary by an inversion. The precise map between the plane and the sphere is given by an inversion around the point $x = \left(\vec{x},\, x_d = -\frac{1}{2}\right)$,

$$x_d = \frac{x'_d + 1}{\left(x'_d+1\right)^2 + \vec{x}'^2} - \frac{1}{2}, \qquad \vec{x} = \frac{\vec{x}'}{\left(x'_d+1\right)^2 + \vec{x}'^2}, \tag{1.84}$$

where x' represent the transformed coordinates under inversion.

In fig. (1.4) we show that the region defined by $x'^2 < 1$ corresponds to the upper half plane $x_d > 0$. Let us denote the coordinates of the sphere using a more standard notation $\vec{r} = (\vec{x}', x'_d)$. This mapping

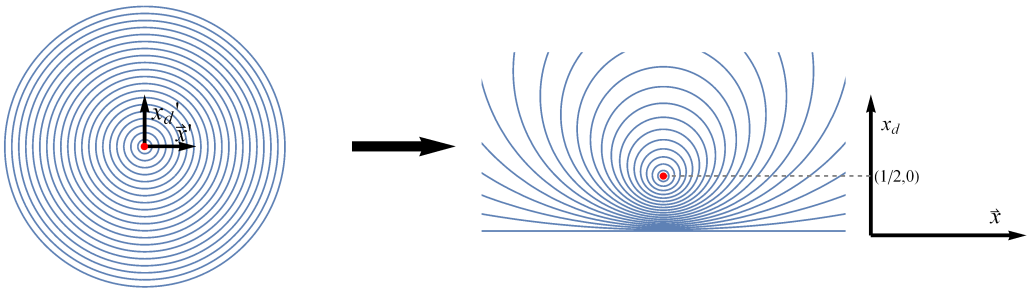

Figure 1.4: Under an inversion, the interior of the sphere is mapped to the upper half space defined by $x_d > 0$.

corresponds to a Weyl transformation, so the correlation functions can be written as:

$$\langle \mathcal{O}(\vec{r}) \rangle = \frac{a}{\left(1 - \left(\frac{\vec{r}}{R}\right)^2\right)^{\Delta}} \frac{1}{R^{\Delta}} \tag{1.85}$$

$$\langle \mathcal{O}_1(\vec{r}_1)\, \mathcal{O}_2(\vec{r}_2) \rangle = \frac{g(\zeta)}{\left[\left(1 - \left(\frac{\vec{r}_1}{R}\right)^2\right)\left(1 - \left(\frac{\vec{r}_2}{R}\right)^2\right)\right]^{\triangle}} \frac{1}{R^{2\triangle}}, \tag{1.86}$$

where the conformal cross ratio ζ is given by

$$\zeta = \frac{\left(1 - \left(\frac{\vec{r}_1}{R}\right)^2\right)\left(1 - \left(\frac{\vec{r}_2}{R}\right)^2\right)}{\left(\frac{\vec{r}_1}{R} - \frac{\vec{r}_2}{R}\right)^2}. \tag{1.87}$$

Notice that in the case of a scale invariant field theory, the one and two point functions are not so constrained. In fact, using just scale symmetry, the one point function of an operator is fixed up to an arbitrary function,

$$\langle \mathcal{O}_{\Delta}(\vec{r}) \rangle = \frac{1}{R^{\Delta}} f\left(\left|\frac{\vec{r}}{R}\right|\right). \tag{1.88}$$

It is only after using the inversion to map to the planar boundary that we can get the result (1.85). The same happens for the two point function. Namely, using just scale symmetry, we can fix it up to,

$$\langle \mathcal{O}_{\Delta_1}(\vec{r}_1)\, \mathcal{O}_{\Delta_2}(\vec{r}_2) \rangle = \frac{1}{R^{\Delta}} f\left(\frac{\vec{r}_1}{R}, \frac{\vec{r}_2}{R}, \frac{\vec{r}_1 \cdot \vec{r}_2}{R^2}\right), \tag{1.89}$$

or, in other words, it can depend on the ratios of $\frac{\vec{r}i}{R}$ and on the angle between the positions $\vec{r}_1$ and

$\vec{r}_2$. Using also inversion symmetry and comparing with the result of the planar boundary we would get (1.86). Thus, we conclude that analyzing the three dimensional Ising model in the presence of a spherical boundary allows to test for the conformal invariance of the critical point.

1.9 Outline of thesis

In the next chapter, we review the main concepts involved in the computational methods, used to perform the Ising simulation. More precisely, we will describe what is importance sampling and detailed balance. Then, we discuss two Monte Carlo methods, the Metropolis and the Wolff algorithms, and point out their main advantages as well as their disadvantages.

In the third chapter, we introduce methods for calculating averages and errors in a Monte Carlo sample. To do this, we appeal to a toy model.

In the fourth chapter, we do an analysis of the phase transition of the 2D and 3D Ising model. For the computational part, we use the material of chapters two and three. For the theoretical part, we use the content of the first chapter. We introduce the concept of the Finite Size Scaling and its importance in the study of critical exponents.

In the fifth chapter we present the results for the computation of the one and two point function in the presence of a spherical boundary. We analyze the data and checked a strong indication of conformal invariance of the three dimensional Ising model.

In the last chapter, we conclude pointing out the main goals of the thesis and possible extensions to this work.

Chapter 2

Monte Carlo methods

One of the most important quantities in Statistical Physics is the partition function, that we usually denote by Z. The partition function is the sum over all possible states that a system can have. The probability distribution of a system to be in a state α is given by the Boltzmann factor, $\exp(-\beta E_\alpha)$, where E_α is the energy of the state α. So, the partition function can be written as

$$Z = \sum_\alpha \exp(-\beta E_\alpha). \tag{2.1}$$

We are able to calculate all other functions that are important to the system, such as its average energy, magnetization, specific heat or magnetic susceptibility, if we know the partition function. There are models whose partition function is exactly calculated - we can mention the Ising Model in one and two dimensions - but, in the majority of the cases, it is not known any exact analytical expression, or even for any other thermodynamic function.

However, generally, it is not easy to calculate analytically the sum of a partition function, since it can have a large number of states. In order to try to overcome this problem, we employ computational methods.

Monte Carlo methods are one of the most used numerical computational methods. They base, precisely, in repetition of a higher number of simulations, with the view to calculate probabilities and average values. With them, we are able to simulate a system that can evolve from one state to another. In fact, the main point of Monte Carlo methods is that it is a trick to generate the correct probability distribution.

In the following we will explain the main ideas behind Monte Carlo methods: importance sampling, Markov processes and detailed balance.

2.1 Review of Monte Carlo Methods

In a real life experiment, to measure a physical quantity, we are just probing a limited amount of the total phase space of the system, since the system does not have time to reach all possible states. In the definition of partition function and of an average of a physical observable, we have a sum over all states of the system. However, most of the times, it is hard to obtain these quantities analytically. Thus, we must find sensible approximations to proceed with a theoretical analysis of the system. As in a real life experiment, some states are more important than other and one approximation scheme is called **importance sampling**.

The idea behind importance sampling is that some states of a simulation have bigger impact in the parameter that is being estimated than others. This is a technique of variance reduction, that is, it allows to increase the accuracy of estimates that we get from iterations. In other words, with this technique we pick the distribution that will favor the accuracy of estimates relatively to the real value. We will see how this works with an example.

Suppose we intend to estimate the mean value of an observable quantity, $\langle M \rangle$(for instance, the magnetization of a system).If the system is small, we can compute exactly the value using the expression for the average:

$$\langle M \rangle = \frac{\sum_\mu M_\mu \exp\left(-\beta E_\mu\right)}{\sum_\mu \exp\left(-\beta E_\mu\right)}, \tag{2.2}$$

On the contrary, when we have huge systems, the best we can do is the average over a set of states. In that way, the estimate for M is:

$$M_N = \frac{\sum_{i=1}^{N} M_{\mu_i} p_{\mu_i}^{-1} \exp\left(-\beta E_{\mu_i}\right)}{\sum_{j=1}^{N} p_{\mu_j}^{-1} \exp\left(-\beta E_{\mu_j}\right)}, \tag{2.3}$$

where M_N is the estimator[1] of M and p_μ is a given distribution. When $N \to \infty$ (large number of samples used to the average), then $M_N = \langle M \rangle$. One of the key points is to choose appropriately the distribution p_μ. Let us consider a simple but inefficient distribution to understand better the importance of this step. Suppose that p_μ is constant and equal for all states. Then, the estimator is given by

$$M_N = \frac{\sum_{i=1}^{N} M_{\mu_i} \exp\left(-\beta E_{\mu_i}\right)}{\sum_{j=1}^{N} \exp\left(-\beta E_{\mu_j}\right)}. \tag{2.4}$$

This method has a drawback, as it favors states which contribute negligibly to the estimate as states with significant contributions. This method would improve if we could insert a bias towards the states that give significant contributions. Let us emphasize that this inefficiency would be more dramatic at low

[1] An estimator is a quantity that allows us to calculate estimates of some values, such as the mean of a population, based on measurements of a sample.

temperatures, where the system can be dominated by few or just one state . To deal with this issue, we choose the probability to be

$$p_\mu = \frac{\exp\left(-\beta E_\mu\right)}{Z}. \tag{2.5}$$

In this case, the estimator M_N is written as

$$\begin{aligned} M_N &= \frac{\sum_{i=1}^{N} M_{\mu_i} \frac{Z}{\exp\left(-\beta E_{\mu_i}\right)} \exp\left(-\beta E_{\mu_i}\right)}{\sum_{j=1}^{N} \frac{Z}{\exp\left(-\beta E_{\mu_j}\right)} \exp\left(-\beta E_{\mu_j}\right)} \\ &= \frac{1}{N} \sum_{i=1}^{N} M_{\mu_i}, \end{aligned} \tag{2.6}$$

where the states μ_i are chosen with probability p_{μ_i}.

Thus, we have just shifted the problem, since now we have to generate a random set of states according to the Boltzmann distribution p_μ. To solve this problem, we use a **Markov process** to create states. The steps involved in Markov process are the following:

- start with a given state i;
- generate, randomly, another state, j;
- Accept the transition from state i to the state j, with probability $P\left(i \to j\right)$.

The probabilities satisfy the completeness condition, $\sum_j P\left(i \to j\right) = 1$. After running the program several times, the system creates states according to the Boltzmann distribution - i.e., the system reaches the equilibrium.

The condition that guarantees that the generated distribution is the Boltzmann distribution, after our system come to equilibrium, is the **detailed balance**. Mathematically, we can write this condition as:

$$p_i P\left(i \to j\right) = p_j P\left(j \to i\right), \tag{2.7}$$

in which p_i is the probability of being in i and p_j is the probability of being in site j, in the stationary regime. These probabilities are of the form (2.5). Basically, (2.7) states that, on average, the system in equilibrium goes $i \to j$ so frequently as it goes $j \to i$.

2.2 Examples of Monte Carlo Methods

After this brief introduction, it is worth to describe two Monte Carlo Methods, that were used to do the present work. They are: Metropolis algorithm and Wolff algorithm.

2.2.1 Metropolis algorithm

The Metropolis algorithm was created by Nicolas Metropolis and collaborators in 1953 [14]. The goal is to get random samples from a certain probability distribution, for which is difficult to directly sample.

According to this method, the states are created from previous states, using the transition probability, that depends on the difference of energies between the final and the initial states.

It is vastly used in Monte Carlo, giving, for example, the possibility of having the thermodynamic quantities of a system of spins. Once that this work focus on Ising Model, let us describe what is the mechanism of the method in a system of spins:

- Choose one spin, randomly, in position i;
- Calculate the difference of energy between initial configuration and the configuration with the spin in the position i inverted: ΔE;
- Generate a random number, r (chosen uniformly in $[0, 1]$);
- If $r < \exp\left(-\frac{\triangle E}{k_B T}\right)$, flip the spin.

Then, we choose another site, calculate again the difference between energies, generate a random number and compare it with the Boltzmann factor, and so on, until reach every spin. This algorithm, that allows to flip a single spin, is said to have single-spin-flip dynamics.

2.2.2 Wolff algorithm

The correlation length of the system increases in the vicinity of the critical point of a phase transition.This induces the formation of domains - group of spins that point in the same direction. Since they have the same orientation, there will be a strong ferromagnetic interaction between pairs and it will be more difficult to flip every spin of the domain. The cost of inverting a spin is $2zJ$, in which z is the coordination number (number of first neighbors). If the spin is in the edge of the domain, it requires less energy to flip. However, using a single-spin-flip algorithm to try to invert the whole domain takes a considerably amount of time. Thus, we need a more efficient way to perform this task.

The Wolff algorithm was proposed by the man with the same name, Ulli Wolff, in 1989 [22], based in works of Swedsen and Wang (1987) [21]. The idea is searching for clusters - i.e., sets of spins which are correlated - and inverting all the cluster at once (and not spin by spin). Algorithms of this type are called cluster-flipping algorithms.

This algorithm satisfies the detailed balance and the probability of adding a spin to the cluster (in the Ising Model) is $P_{add} = 1 - \exp\left(-2\beta J\right)$.

The recipe for Wolff algorithm is the following:

- Choose a spin, randomly, from the lattice;
- Verify the neighbors. If they are pointing in the same direction, they can be added to the cluster with probability P_{add}. If not, they are not added to the cluster.
- For every added spin, check out its neighbors and, if they have the same orientation, add them with probability P_{add}. Notice that it is possible to have spins that we checked but they already belong to the cluster; in this case, we will not add it again. On the other hand, we can be testing spins that have been tested before, but were rejected with probability $1-P_{add}$. In these conditions, they can have now the possibility of joining the cluster. This process is repeated until every spin is tested.
- Finally, invert the cluster.

2.3 Metropolis vs Wolff Algorithms

In spite of being more complex to implement than Metropolis algorithm, we will see that the Wolff algorithm provides accurate results in the region that we are interested in: the critical region. However, Wolff method is slower than Metropolis algorithm both at high and low temperatures.

When the temperature is very high, the spins, generally, are not aligned in the same direction. For this reason, most of the times, the cluster is just one spin. In this way, the Wolff algorithm only inverts one spin - and that is exactly what Metropolis algorithm does. Nevertheless, the Wollf is slower because it will check the alignment of every neighbor spin, while Metropolis only has to decide when to flip.

If the temperature is low, P_{add} is very high, because almost every spins point in the same direction. Therefore, it is probable to choose a spin and all its neighbors are aligned like it. The cluster becomes huge and can occupy all the lattice. Consequently, the large cluster (or all lattice) is inverted only once, after the checking of every neighbor, that costs time.

How can we know that Wolff algorithm is better in critical region? How can we quantify it? In order to understand this, let us introduce the quantity z, called dynamic exponent.

Let us remark that the exponent z is not an universal exponent, because it depends on the algorithm we are using to do the simulation. For temperatures near the critical temperature, the autocorrelation time, τ, that is the time needed for the system to loose memory of the initial state[2], goes with the length of the lattice in this way:

$$\tau \propto L^{d+z}, \tag{2.8}$$

[2]This is a poor explanation of what really is the autocorrelation time. Nevertheless, it will become clear in chapter 3.

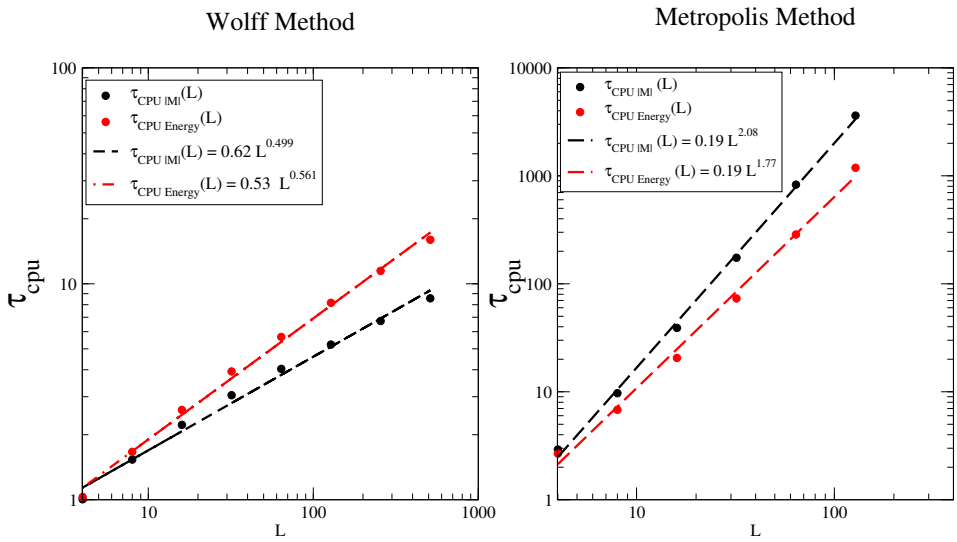

Figure 2.1: τ_{CPU} for absolute magnetization and for energy, depending on L, for $2D$ Ising Model, using different algorithms: Wolff and Metropolis. It was used the T_c of $2D$ Ising Model. The points are the experimental measurements and the dotted line is a power regression of data.

where d is the dimensionality of the system. This power law dependence is very common in critical phenomena.

A large value of z indicates that, as we approximate the critical temperature, the simulation is slower and less accurate. On the contrary, a small z indicates a small critical slowing down and a faster algorithm. $z = 0$ means that there is no critical slowing down and the corresponding algorithm can be used until the critical temperature, without τ becoming very large. The critical slowing down is an abnormal growth of the autocorrelation time close to the critical temperature.

Notice that we must be very careful in order to be fair to measure the autocorrelation time in Metropolis and Wolff methods. For Metropolis algorithm, the computation time is the same at any temperature and is given by:

$$\tau_{CPU} = \frac{\tau}{L^d}, \tag{2.9}$$

i.e., is measured in Monte Carlo Steps (MCS): $1\,MCS \equiv L^d$. It is the best choice for measure because, to uncorrelate all spins in Metropolis algorithm, we need to run the simulation at least L^d, that is, the size of the lattice.

In the case of Wolff algorithm, the computation time varies with temperature. Thus, in the computation of τ_{CPU} , beyond the autocorrelation time of the system, we have to take into account the time needed to execute a step of Markov chain. This is proportional to the average number of tested spins (for each temperature):

$$\tau_{CPU} = \tau \frac{\eta_\beta}{L^d}, \tag{2.10}$$

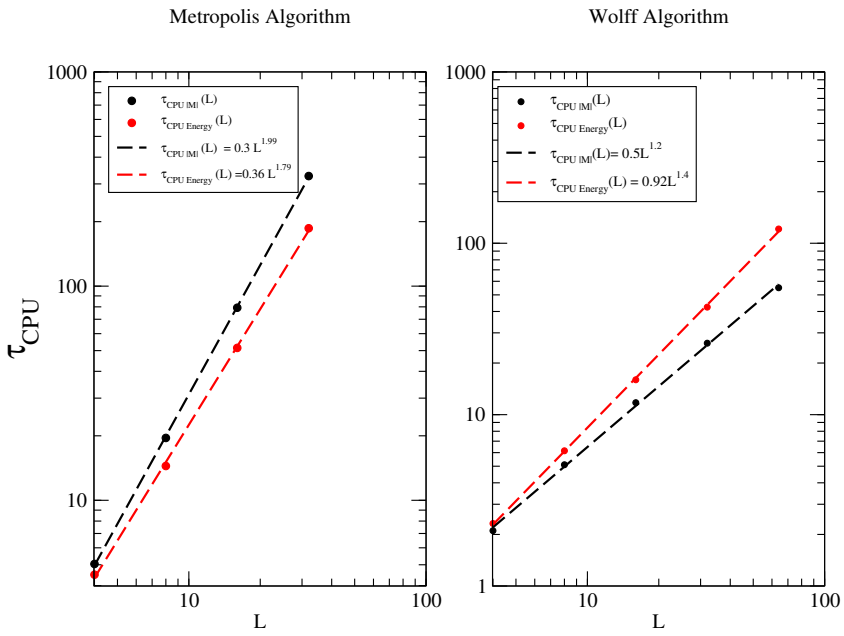

Figure 2.2: τ_{CPU} for absolute magnetization and for energy, depending on L, for $3D$ Ising Model, using different algorithms: Wolff and Metropolis. It was used the T_c of $3D$ Ising Model. The points are the experimental measurements and the dotted line is a power regression of data.

in which η_β is the number of flipped spins.

Studying the τ_{CPU} for different size systems, for $2D$ Ising Model, we obtained the plot of fig.(2.1). In graph (2.1), we can observe the τ_{CPU} for the $2D$ Ising Model, with two different algorithms, for different lattice sizes: 4^2, 8^2, 16^2, 32^2, 64^2, 128^2, 256^2, 512^2 for Wolff algorithm and 4^2, 8^2, 16^2, 32^2, 64^2, 128^2, 256^2 for Metropolis. We performed measurements of τ_{CPU} in the calculation of absolute magnetization and average energy of the system. In both cases, we find that z is lower for the Wolff technique, which means that it is better than Metropolis in measuring near critical temperature. It costs less CPU time. The time scale for the simulation is the higher autocorrelation time measured; in this case, it is $\tau_{CPU\,E}$ for Wolff algorithm and $\tau_{CPU\,|M|}$for Metropolis algorithm.

In the literature, we can find different measures of z, using a wide variety of methods of measurement. The range of values for algorithms that flips only one spin at a time, such as the Metropolis, varies between $z = 1.7$ and $z = 2.7$. The reference value, till the moment, for z, for these type of algorithms, was calculated by Nightingale and Blöte in 1996 [17] , and is $z = 2.1665 \pm 0.0012$. In the case of z_{Wolff}, the best calculation belongs to Coddington and Baillie (1992) [7] and is $z_{Wolff} = 0.25 \pm 0.01$. For Metropolis algorithm, we find $z = 2.08$ and for Wolff $z_{Wolff} = 0.561$. In the plot (2.1) , for Wollf algorithm, it is possible to note a slight curvature of the data. If we calculate the autocorrelation time for larger systems, probably, the dynamic exponent will decrease, reaching the tabulated values, or even

correct them. It was not done because it takes too much time to get z values for higher systems.

In any case, the value of z is smaller for Wolff algorithm, so, it is the best method to use near critical temperature. Once that the present work studies the critical region, in all measurements, we use the Wolff algorithm.

For the 3D Ising Model, in the literature, the value of z is 2.08 [15] , using the Metropolis algorithm. In the case of using the Wolff algorithm, the value of z is 0.44 [8]. In fig.(2.2), we performed a measurement of z using both algorithms.

We used lattices of size 4^3, 8^3, 16^3 and 32^3 for Metropolis and lattices of size 4^3, 8^3, 16^3, 32^3 and 64^3 for Wolff. τ_{CPU} was calculated using the estimate of critical temperature for the $3D$ Ising Model, that is $\beta_{C\,3D} = 0.2216595$ [11]. We find that $z = 1.99$ for Metropolis algorithm and that $z = 1.4$ for Wolff Algorithm.

Chapter 3

Averages and errors in a Markov chain Monte Carlo sample

This chapter is an introduction to error theory in Monte Carlo methods. We chose a toy model to apply the techniques, in order to understand how we calculate the averages and errors. The interested reader can find more information in references [1],[24].

3.1 Definitions

Assume that we have a series of data points generated by a Monte Carlo process in equilibrium:

- the probability of each event is independent of time;
- the probability of a pair of events, one at time t_i and other at t_{i+m}, only depends on the difference of time: $t = t_{i+m} - t_i$.

The moments for each value of x_t are given by the equilibrium probability distribution, $P(x)$,

$$\langle x_t^n \rangle \quad = \quad \langle x^n \rangle = \int dx x^n P(x) . \tag{3.1}$$

It is useful to define the covariance between two variables,

$$\chi_{xy} = \langle xy \rangle - \langle x \rangle \langle y \rangle , \tag{3.2}$$

and the cross averages involving different times,

$$\begin{aligned}\langle x_{t_1} y_{t_2}\rangle &= \int dx \int dy\, xyP\left(x,t_1;y,t_2\right) \\ &= \int dx \int dy\, xyP\left(y,t_2|x,t_1\right)P\left(x,t_1\right), \end{aligned} \tag{3.3}$$

If we are dealing with a Markov process in equilibrium:

$$P\left(x_1,t_1\right) = P\left(x\right) \tag{3.4}$$

$$P\left(y,t_2|x,t_1\right) = P\left(y,\left(t_2-t_1\right)|x,0\right), \tag{3.5}$$

that is, the average $\langle x_{t_1} y_{t_2}\rangle$ only depends on the difference of time.

If the Markov process respects the detailed balance,

$$P\left(y,t_2|x,t_1\right)P\left(x\right) = P\left(x,t_2|y,t_1\right)P\left(y\right), \tag{3.6}$$

and we get

$$\langle x_{t_1} y_{t_2}\rangle = \langle y_{t_1} x_{t_2}\rangle = \langle xy\rangle\left(t_2-t_1\right). \tag{3.7}$$

Other important quantity is the normalized correlation function:

$$C_{xy}\left(t\right) = \frac{\langle xy\rangle\left(t\right) - \langle y\rangle\langle x\rangle}{\chi_{xy}}. \tag{3.8}$$

The autocorrelation time is the sum over all instants of the correlation function:

$$\tau = \sum_{t=1}^{\infty} C\left(t\right). \tag{3.9}$$

These general statements will be useful to understand the next sections.

3.2 Toy model of correlated data

The aim of a toy model is to use a simpler model to understand more complex systems. It allows us to calculate some properties and verify them easily, so that we can know if we are in the right direction. The chosen toy model is the one dimensional (1D) random walk “in a box”, with periodic boundary conditions, that is described below.

Suppose that we have a 1D box of length L and periodic boundary conditions, i.e., we can identify $L \equiv 0$ (see fig. (3.1)). The walker is allowed to walk a path of T steps in the box, but with some

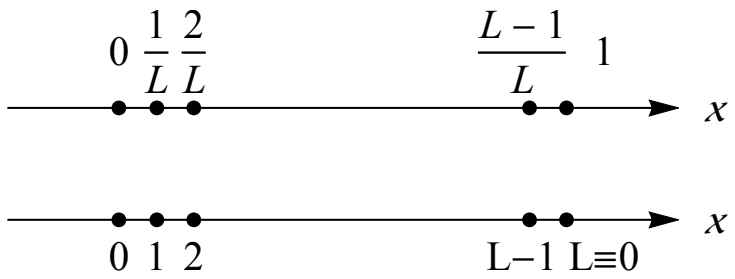

Figure 3.1: Representation of the path of the walker. Notice that we normalize the positions by the length (L) of the "box".

conditions: he can walk one step to the right with probability p_r, one step to the left with probability p_l or stay in the same spot with probability p_s. If we enable the walker to take a large number of steps, in the end, what happens is that the probability of being in any spot in the box is the same. In other words, the system reaches the asymptotic limit. In this case, the probability is:

$$p = \frac{1}{L}. \tag{3.10}$$

Therefore, in the equilibrium, the mean value of the position in which the walker can be is given by:

$$\begin{aligned} \langle x \rangle &= \sum_{k=0}^{L-1} \frac{k}{(L-1)} p \\ &= \sum_{k=0}^{L-1} \frac{k}{(L-1)} \frac{1}{L} \\ &= \frac{1}{2}, \end{aligned} \tag{3.11}$$

where we divided the positions by the size of the system. The mean value for x^2 is:

$$\left\langle x^2 \right\rangle = \sum_{k=0}^{L-1} \left(\frac{k}{(L-1)} \right) p = \frac{1}{6} \frac{(2L-1)}{(L-1)}. \tag{3.12}$$

Thus, with (3.11) and (3.12), we can build the variance for the system in equilibrium:

$$\left\langle x^2 \right\rangle - \langle x \rangle^2 = \frac{1}{6} \frac{(2L-1)}{(L-1)} - \frac{1}{4}. \tag{3.13}$$

In the following sections, we will test these equations.

3.2.1 Analytical evolution in time

The goals of using this toy model are: study it in an analytical way, since it can be solved exactly; perform simulations and compare them with the results provided by the exact solution; and, in the next sections, use the data from simulations to illustrate some results of error theory.

For the system of the 1D random in a box with periodical boundary conditions, the master equation that governs the temporal evolution of probability of being in a position k, P_k, (do not forget that we are considering only the transitions between first neighbor positions) is:

$$\begin{cases} P_0\left(t+1\right) = p_l P_1\left(t\right) + p_r P_{L-1}\left(t\right) + \left(1-p_r-p_l\right) P_0 \\ P_k\left(t+1\right) = p_l P_{k+1}\left(t\right) + p_r P_{k-1}\left(t\right) + \left(1-p_r-p_l\right) P_k\left(t\right), \quad 0 < k < L-1 \\ P_{L-1}\left(t+1\right) = p_l P_0\left(t\right) + p_r P_{L-2}\left(t\right) + \left(1-p_r-p_l\right) P_{L-1} \end{cases}. \tag{3.14}$$

With this system of equations, we are able to construct a matrix - the Markov matrix, Ω_{ij}. In this way, we have a rule to relate the positions of the walker at instants t and $t+1$:

$$P_i\left(t+1\right) = \sum_j \Omega_{ij} P_j\left(t\right). \tag{3.15}$$

This Markov matrix is of the form:

$$\begin{pmatrix} (1-p_r-p_l) & p_l & 0 & \dots & p_r \\ p_r & (1-p_r-p_l) & \dots & \dots & 0 \\ 0 & \vdots & \ddots & & \\ \vdots & & & \ddots & \\ p_l & & & p_r & (1-p_r-p_l) \end{pmatrix}. \tag{3.16}$$

The calculation of eigenvectors and eigenvalues of the Markov matrix will be determinative for getting the correlation function between two points separated in time, as we will see in (3.30).

The equation for eigenvalues and eigenvectors is:

$$\Omega_{ij}\varphi_j = \lambda\varphi_j. \tag{3.17}$$

To simplify, we assume that it is a diffusion process. In a diffusion process, the velocity of a given particle is zero; however, in this particular case of study, we do not deal with velocities, but with probabilities. Thus, for a diffusion process in a random walk, $p_r = p_l$. Notice that if, for instance, $p_r > p_l$, the walker would move more often to the right than to the left. To simplify the notation, let us write $p_r = p_l = p$.

Note that there are right eigenvectors, as in (3.17), and left eigenvectors. Generally, they are not the

same. However, in this specific case, once that Ω_{ij} is symmetric (because $p_r = p_l$), the left and right eigenvectors are the same.

In this way, the system (3.17) is:

$$\begin{cases} \lambda\varphi_0 = p\varphi_1 + p\varphi_{N-1} + (1-2p)\,\varphi_0 \\ \lambda\varphi_k = p\varphi_{k+1} + p\varphi_{k-1} + (1-2p)\,\varphi_k, \qquad 0 < k < L-1 \\ \lambda\varphi_{L-1} = p\varphi_0 + p\varphi_{L-2} + (1-2p)\,\varphi_{L-1} \end{cases} \tag{3.18}$$

Considering the periodic boundary conditions and that the component j of φ, the eigenvector, is of the form

$$\varphi_j^k = \exp\left(i\frac{2\pi}{L}kj\right), \tag{3.19}$$

we get the expression for the spectrum of eigenvalues:

$$\lambda_k = 1 - 2p + 2p\cos\left(\frac{2\pi}{L}k\right). \tag{3.20}$$

Here, $\lambda_k = \lambda_{L+k} = \lambda_{-k} = \lambda_{L-k}$ and $k \in \{0, 1, ..., L-1\}$.

Remark that it is possible to write the probability of being in position j at instant $t = 0$, $P_j\,(0)$, as a linear combination of its eigenvectors:

$$P_j\,(0) = \sum_{k=1}^{\infty} a_k \varphi_j^k. \tag{3.21}$$

So, the challenge is now to find the a_k coefficients. To do that, we have to apply the inner product:

$$\sum_j \left(\varphi_j^{k'}\right)^* P_j\,(0) = \sum_{k\in S}\sum_j a_k \left(\varphi_j^{k'}\right)^* \varphi_j^k, \tag{3.22}$$

where the $*$ denotes the complex conjugate. The expression to the a_k coefficients is:

$$a_{k'} = \frac{\sum_j \left(\varphi_j^{k'}\right)^* P_j\,(0)}{L}. \tag{3.23}$$

Moreover, it is possible to write Ω^n in this way:

$$\Omega^n = S^{-1} D^n S, \tag{3.24}$$

where S^{-1} is the vector of transposed eigenvectors of Ω, D is a matrix of respective eigenvalues

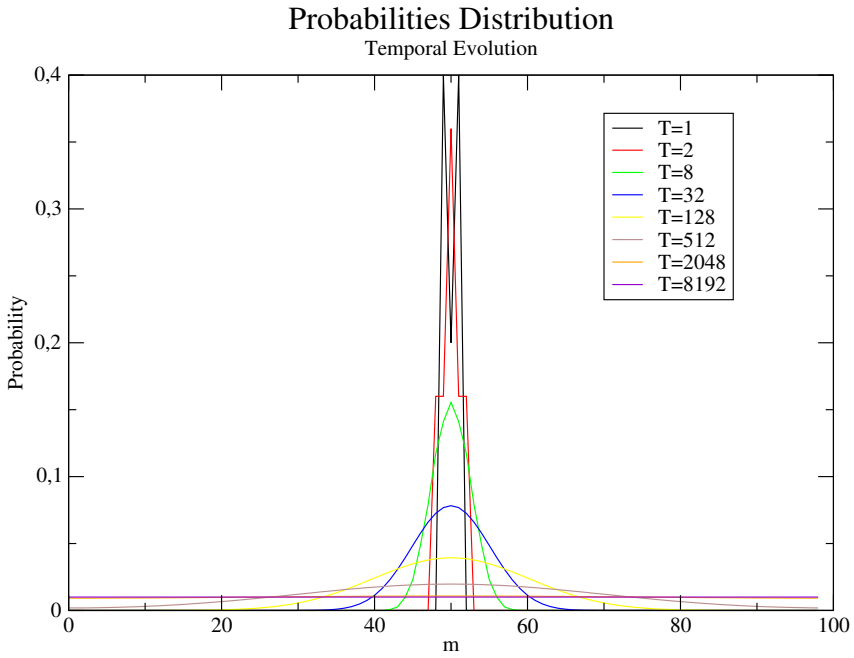

Figure 3.2: Evolution with time for $P(m,t|l,0)$, with a box of $L = 100$ and $p = 0.3$, starting in $l = \frac{L}{2}$. T is the number of steps of the walker. In this plot, we do not normalize the positions by the size of the system. Therefore, $p_{equilibirum} = 0.01$.

and S is the vector of eigenvectors. Therefore, we achieve:

$$\left[\Omega^t\right]_{lm} = \frac{1}{L}\sum_{k=0}^{L-1} \exp\left(\frac{i2\pi k\,(m-l)}{L}\right)\lambda_k^t. \tag{3.25}$$

If we are interested in calculate the probability of being in a position m, at instant t, knowing that the walker was in a position l at instant 0, $P(m,t|l,0)$, we have to do:

$$P(m,t|l,0) = \left[\Omega^t\right]_{ml}. \tag{3.26}$$

We can observe that, when $t \to \infty$, the probability approaches to the value given by (3.10), that is the asymptotic limit. Once again, this happens because the case in study is diffusive. Thus, starting from any initial position, the diffusion will spread the probability for all positions. Since there is a limited number of positions, this process will converge in a uniform distribution.

In graph (3.2), we can observe the distribution of probabilities, evolving with time. Notice that, as time increases, the distribution becomes more and more soft, and culminates in a uniform distribution, as expected.

3.2.2 Autocorrelation Dynamics

Now, we will focus on the analytical study of the autocorrelation function of positions and the autocorrelation time for this system. The autocorrelation function of positions, $C(n)$, is defined as the way that a position at time t is related with itself at time $t+n$. The autocorrelation time, τ, is the time needed to uncorrelate the positions at different instants of time. The mathematical expressions are, recalling (3.8) and (3.9):

$$C(n) = \frac{\langle x\,(t)\; x\,(t+n)\rangle - \langle x\,(t)\rangle \langle x\,(t+n)\rangle}{\langle x^2\,(t)\rangle - \langle x\,(t)\rangle^2} \tag{3.27}$$

$$\tau = \sum_{n=1}^{\infty} C\,(n)\,. \tag{3.28}$$

In order to calculate the correlation function (3.27), we should compute $\langle x\,(t)\; x\,(t+n)\rangle$ (we know $\langle x\,(t)\rangle$ and $\langle x\,(t+n)\rangle$ from (3.11) and $\left\langle x^2\,(t)\right\rangle - \langle x\,(t)\rangle^2$ from (3.13)) .

First of all, the expression for $\langle x\,(t)\; x\,(t+n)\rangle$ is:

$$\langle x\,(t)\; x\,(t+n)\rangle \;=\; \sum_{l=0}^{L-1} \frac{l}{(L-1)} p_l \sum_{m=0}^{L-1} \frac{m}{(L-1)} p_m \tag{3.29}$$

In this way, we are able to do:

$$\langle x\,(t)\; x\,(t+n)\rangle = \frac{1}{L} \sum_{l,m=0}^{L-1} \frac{l}{(L-1)} \frac{1}{L} \frac{m}{(L-1)} \sum_{k=0}^{L-1} \exp\left(\frac{i2\pi k\,(m-l)}{L}\right) \lambda_k^n. \tag{3.30}$$

For the case $k=0$, we get (see in (3.20) that $\lambda_0 = 1$):

$$\frac{1}{(L-1)^2 L^2} \sum_{l,m=0}^{L-1} lm = \frac{1}{4}. \tag{3.31}$$

So, the expression for (3.27) is:

$$C(n) \;=\; \frac{\frac{1}{4} + \sum_{k=1}^{L-1} \frac{\lambda_k^n}{\sin^2\left(\frac{\pi k}{L}\right)} - \frac{1}{4}}{\frac{1}{6}\frac{(2L-1)}{(L-1)} - \frac{1}{4}} \tag{3.32}$$

$$\;=\; \frac{3}{L^2-1} \sum_{k=1}^{L-1} \frac{\lambda_k^n}{\sin^2\left(\frac{\pi k}{L}\right)}. \tag{3.33}$$

In turn, the autocorrelation time is given by:

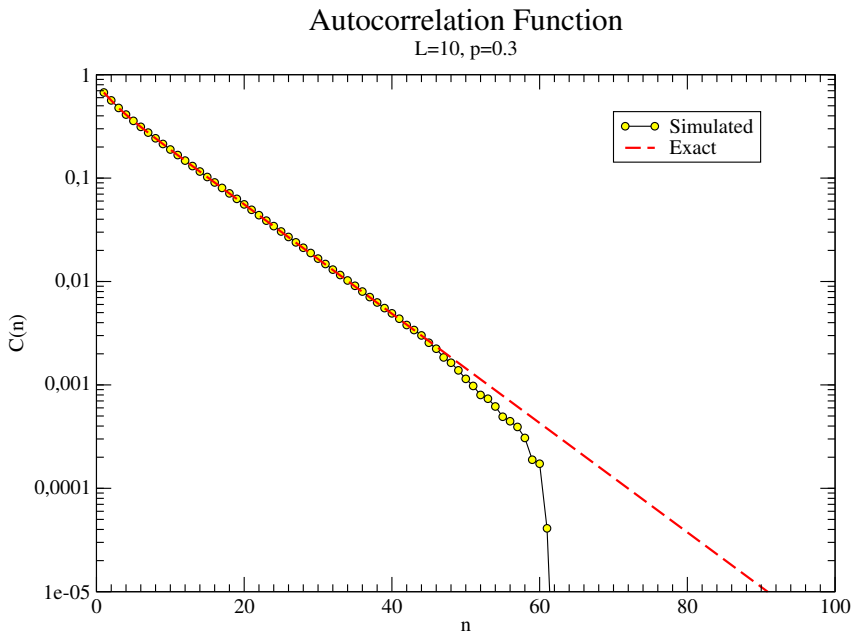

Figure 3.3: Autocorrelation function.

$$\begin{aligned}\tau &= \tfrac{3}{L^2-1} \sum_{k=1}^{L-1}\sum_{n=1}^{\infty} \frac{\lambda_k^n}{\sin^2\left(\frac{\pi k}{L}\right)} \\ &= \frac{3}{L^2-1}\sum_{k=1}^{L-1} \frac{\lambda_k}{\sin^2\left(\frac{\pi k}{L}\right)(1-\lambda_k)} \\ &= \frac{11+L^2-60p}{60p}. \end{aligned} \tag{3.34}$$

We can, also, compute another quantity, which we call γ, and we define by:

$$\gamma = \sum_{n=1}^{\infty} nC(n) \tag{3.35}$$

$$= \frac{3}{L^2-1}\sum_{k=1}^{L-1}\sum_{n=1}^{\infty} \frac{n\lambda_k^n}{\sin^2\left(\frac{\pi k}{L}\right)} \tag{3.36}$$

$$= \frac{\left(L^2-1\right)\left(27+2\left(L^2-1\right)-84p\right)+72\left(3-14p\right)}{5040p^2} \tag{3.37}$$

For a box of $L = 10$ and $p = 0.3$, we get the fig.(3.3). In the plot (3.3), we can observe the auto-

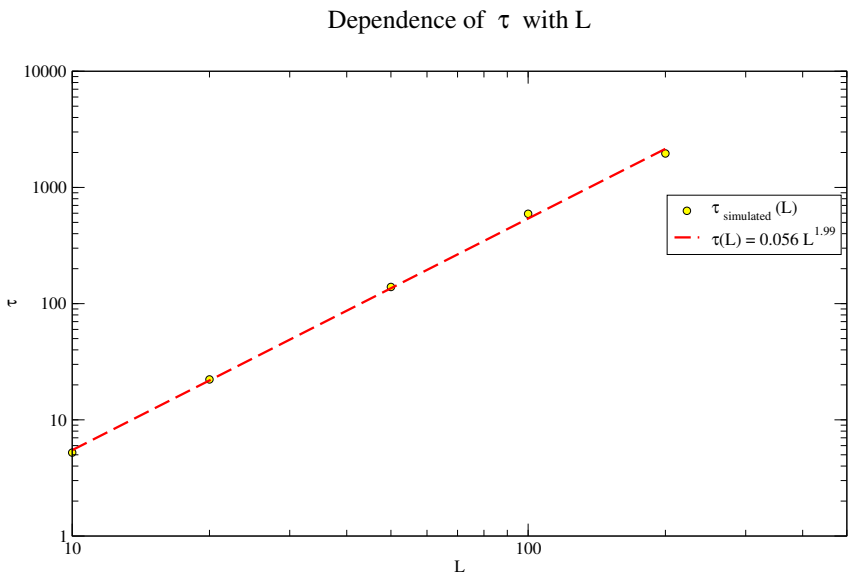

Figure 3.4: Autocorrelation time depending on the length of the box.

correlation function for the positions of walker in different instants of time. The axes are in logarithmic scale. We can infer that the simulation generated with a computational program agrees with theoretical prediction. For large n, the concordance is not very good, due the lack of statistic. When one integrates this function, according to (3.34), one gets the autocorrelation time.

We can verify how autocorrelation time depends on the length of the box, in fig.(3.4).In graph (3.4) we find that $\tau \sim L^2$, that agrees with the analytical prediction. In fact, if we compare with (3.34), the constant of the L^2 is $\frac{1}{60\times 0.3} \sim 0,0556$. Beyond that, this is an expected result, since it is a diffusive process.

3.3 Estimation of statistical quantities

As it was emphasized in the chapter 2, the estimators give us an accurate value of the quantity that we are measuring, for a large sample of data.

In this section, we intend to investigate which is the best estimator for the mean value, the variance and the kurtosis (we will introduce this quantity later, in this subsection) for the data obtained from toy model. The other goals are to find the error in estimation of these quantities and show the more efficient way to implement the estimator calculation in the computer program, i.e., to get the recurrence equations for the mean value, variance and kurtosis.

3.3.1 Mean Value

3.3.1.1 Estimator

Let us find an estimator for the mean value, $\langle x^n \rangle$. We can estimate $\langle x^n \rangle$ for a sample of m points:

$$X_n\left(x^n\right) = \frac{1}{m}\sum_{t=1}^{m} x_t^n. \tag{3.38}$$

X_n is the estimator for the mean value. Notice that X_n is a good estimator for the mean value, since it converges to the correspondent mean value, independently of the correlations between the different samples of x. If we perform the average of X_n, we obtain:

$$\langle X_n\left(x^n\right)\rangle = \frac{1}{m}\sum_{t=1}^{m}\langle x_t^n\rangle = \langle x^n\rangle, \tag{3.39}$$

where we used the fact that the distribution is stationary and, so, independent of t.

If we want to get the average of two different positions temporally separated, $\langle xy\rangle(t)$, we can build the estimator and do its average:

$$\begin{aligned} X\left(xy,\alpha\right) &= \frac{1}{m-\alpha}\sum_{t=1}^{m-\alpha} x_t y_{t+\alpha} \\ \langle X_n\left(xy,\alpha\right)\rangle &= \langle xy\rangle(t) = \chi_{xy}C_{xy}(t) + \langle x\rangle\langle y\rangle. \end{aligned} \tag{3.40}$$

Remark that, with a time series of m points, we can average only over $m-\alpha$ points, due to temporal separation.

3.3.1.2 Error of the average estimation

One way to know what is the error that we are committing in the measure of a quantity is to calculate the average deviation between the estimator and the exact value of the quantity:

$$\left\langle \left(X_n(m) - \langle x^n\rangle\right)^2 \right\rangle, \tag{3.41}$$

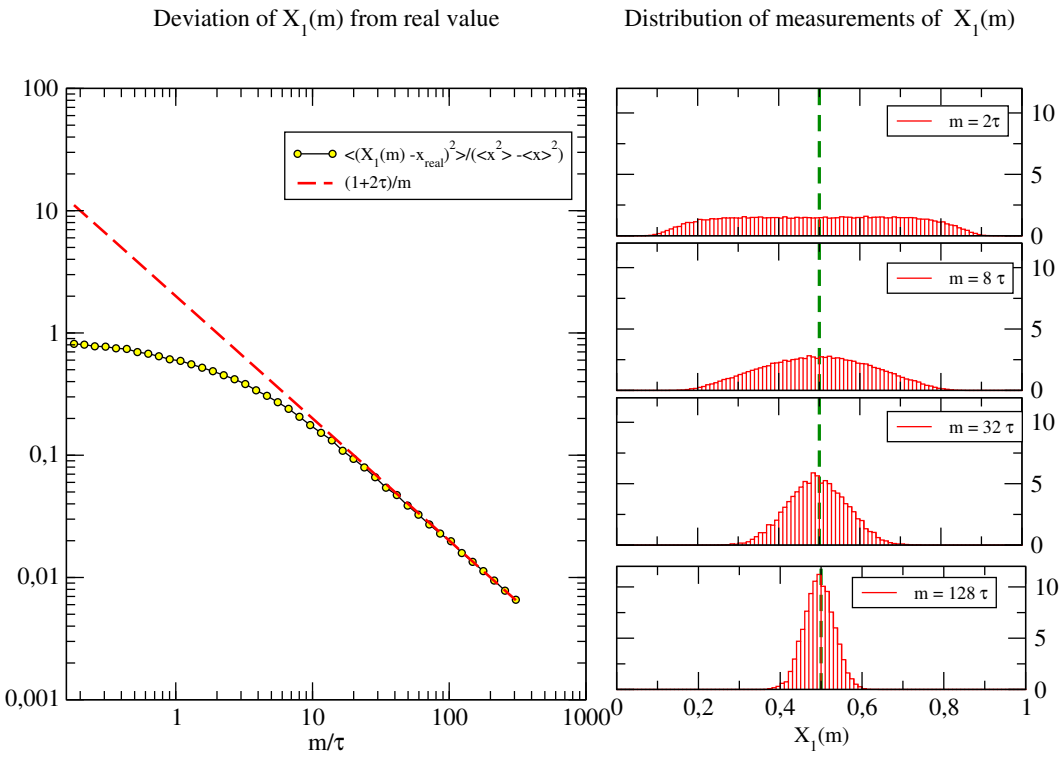

Figure 3.5: Left-hand side: Comparison between left-hand side and right-hand side of (3.42). Right-hand side: using different number of points (m), proportional to τ , we get the distribution of measurements of $X_1\,(m)$. The data was obtained using a box of length $L = 100$ and $p = 0.3$.

in which $\langle x^n \rangle$ is the exact value for the mean. Therefore, the deviation from exact value can be estimated like that:

$$\begin{aligned}
\left\langle \left(X_n\,(m) - \langle x^n \rangle\right)^2 \right\rangle &= \left\langle X_n^2\,(m) \right\rangle - \langle x^n \rangle^2 \\
&= \frac{1}{m^2} \sum_{i,j=1}^{m} \left\langle x_i^n x_j^n \right\rangle - \langle x^n \rangle^2 \\
&= \frac{\chi_{x^n x^n}}{m^2} \sum_{i,j=1}^{m} C_{x^n x^n}\,(i-j) \\
&= \frac{\chi_{x^n x^n}}{m} \left(1 + \frac{2}{m} \sum_{t=1}^{m-1} \sum_{i=t+1}^{m} C_{x^n x^n}\,(t)\right) \\
&\approx \frac{\left\langle x^{2n} \right\rangle - \langle x^n \rangle^2}{m} \left(1 + 2\tau\,(x^n, x^n)\right),\ m \gg \tau
\end{aligned} \tag{3.42}$$

where $t = i - j$.

We can get a graph to compare the right-hand side and the left-hand side of (3.42) and confirm its validity. We will use $n = 1$, which corresponds to $\langle x \rangle$. From the fig. (3.5), we can draw some conclusions. On the left-hand side, when m is small, there is no coincidence between the two functions. This is the regime where $m \ll \tau$, and remember that (3.42) is only valid when $m \gg \tau$. In fact, we can verify that, as we increase m, the two curves get closer. On the right-hand side, we see that, as the number of measurements increases, the value of X_1 is becoming more accurate; there are more measurements whose value is near 0.5, that is the real value for the mean value.

It is quite interesting to analyze the limits of (3.42):

- $\tau = 0$: this case is the standard result of m independent samples, where the error of the mean is the standard deviation of the quantity divided by $\sqrt{m}$.

- $m \gg \tau$: The error still decreases with $\sqrt{m}$, because $\tau\left(x^n, x^n\right)$ is independent of m. Notice that

$$\tau\left(x^n, x^n\right) \approx \frac{1}{m} \sum_{t=1}^{m-1} \sum_{i=t+1}^{m} C_{x^n x^n}(t), \; if \; m \gg \tau. \tag{3.43}$$

  Within this limit, we can extrapolate the limits to infinity, due to the exponential decay of the correlation, and we get:

$$\tau\left(x^n, x^n\right) = \sum_{i=1}^{\infty} C_{x^n x^n}(i), \tag{3.44}$$

that is the definition of τ (see (3.9)).

- $\tau \gg m \gg 1$: here, the error of the mean is basically the standard deviation of x, because the correlation is approximately one. Averaging highly correlated measures does not decrease the error: it is exactly the same of having only one measure.

Another nice interpretation of (3.42) is that, even if we make N averages, due to the correlations, all the measures in groups of size $2\tau + 1$ are correlated. The effective number of independent samples is $m' = \frac{m}{(2\tau+1)}$ or, if we have the same data and only harvesting for the mean value in a longer time interval $(2\tau + 1)$, we will have the same error bar.

3.3.1.3 Recursion for the mean value estimator

The estimator of the mean value is given by (3.38).

The expression for $m + 1$ terms can be written at the expense of the m previous terms. Thus, we

reach a recurrence relation:

$$\begin{aligned} X_n(m+1) &= \frac{1}{m+1}\sum_{i=1}^{m+1} x_i^n \\ &= X_n(m) + \frac{x_{m+1}^n - X_n(m)}{m+1}. \end{aligned} \tag{3.45}$$

This recursion prevents the loss of precision present in (3.38).

3.3.2 Variance

3.3.2.1 Estimator

The variance is given by $\langle x^2\rangle - \langle x\rangle^2$ (it is (3.2) when $x = y$). For convenience, let us set $\sigma^2 = \chi_{xx}$, that is the real value for the variance. We can think that a natural estimator should substitute both averages by their estimators,

$$E_m\left(\sigma^2\right) = X_2(m) - X_1(m)^2, \tag{3.46}$$

in which E_m denotes estimator. However, when one does the average of estimator (3.46), one gets:

$$\begin{aligned} \left\langle X_2(m) - X_1^2(m)\right\rangle &= \frac{1}{m}\sum_{i=1}^{m}\left\langle x_i^2\right\rangle - \langle x\rangle^2 - \frac{\chi_{xx}}{m^2}\sum_{ij} C_{xx}(i-j) \\ &= \chi_{xx} - \frac{\chi_{xx}}{m^2}\sum_{ij} C_{xx}(i-j) \\ &= \chi_{xx}\left(1 - \frac{1+2\tau(x,x)}{m}\right). \end{aligned} \tag{3.47}$$

From (3.47), we conclude that, in fact, the best estimator is:

$$E_m\left(\sigma^2\right) = \frac{m}{m-1-2\tau(x,x)}\left(X_2(m) - X_1^2(m)\right). \tag{3.48}$$

Notice that the factor $\frac{m}{m-1-2\tau(x,x)}$ tends to a constant in the limit of large m:

$$\lim_{m\to+\infty}\frac{m}{m-1-2\tau(x,x)}\left(X_2(m) - X_1^2(m)\right) = \lim_{m\to+\infty}\left(X_2(m) - X_1^2(m)\right). \tag{3.49}$$

It is possible to build a graph to investigate the validity of (3.47). In the left-hand side of the plot (3.6), we see that, if we increase m, the ratio between the measured variance and the exact variance approaches to 1. For small m, the discrepancy is bigger. On the right-hand side, as the number of measurements increase, we get an accurate value of σ^2.

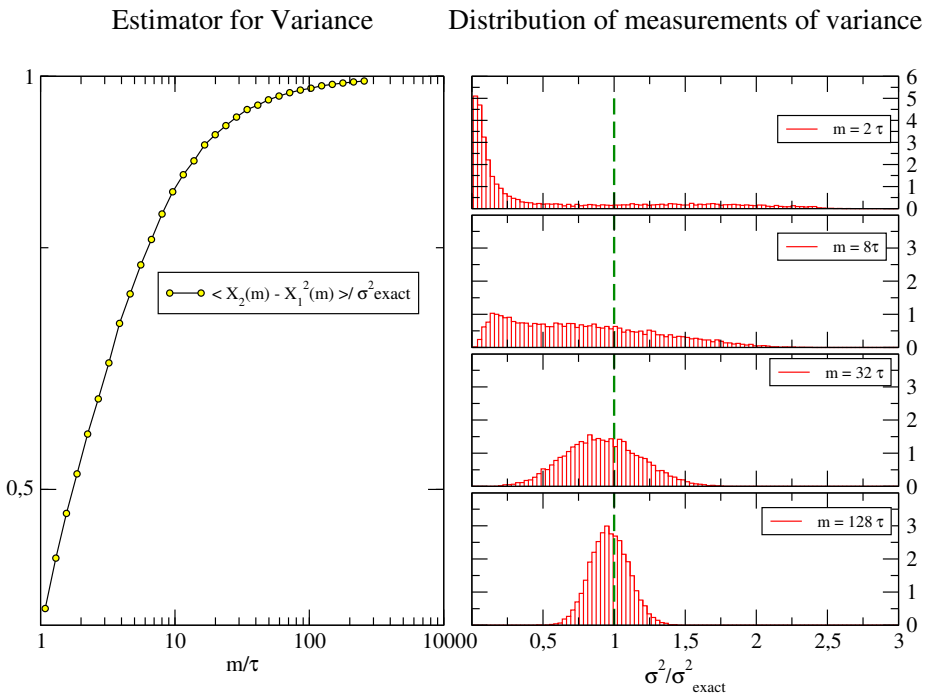

Figure 3.6: Left-hand side: validity of (3.47). Right-hand side: distribution of measurements of σ^2, using different values for m. This data was obtained using a box of length $L = 100$ and $p = 0.3$.

3.3.2.2 Error of the variance estimation

The error of the variance estimation is quite a complicated formula to get an useful implementation of the estimation error, once it involves not only time correlations of two instants, but also three and four point correlations in time.

For this reason, we will introduce, in subsection 3.3.4, a methodology of splitting the data into blocks. It will be useful for estimating the error of the variance estimation.

3.3.2.3 Recursion for the variance estimator

In the sub-subsection 3.3.2.1, we verify that the best estimator for the variance is (3.48). However, in our computational implementations, we need a high value of variance measurements. Thus, when m is very large,

$$E_m\left(\sigma^2\right) \approx X_2\left(m\right) - X_1^2\left(m\right). \tag{3.50}$$

This expression leads to a loss of precision due the finite number of digits in the numerical implementation and, many times, the direct implementation leads to a negative value. To overcome these problems, we proceed identically to (3.45). We write an expression to the $m+1$ having into account the first m

terms:

$$\begin{aligned}\sigma^2(m+1) &= \frac{m}{m+1}X_2(m) + \frac{x_{m+1}^2}{m+1} - X_1^2(m+1) \\ &= \frac{m}{m+1}\sigma^2(m) + \frac{m}{m+1}X_1^2(m) + \frac{x_{m+1}^2}{m+1} - X_1^2(m+1) \\ &= \frac{m}{m+1}\sigma^2(m) - \left(X_1^2(m+1) - X_1^2(m)\right) + \frac{x_{m+1}^2 - X_1^2(m)}{m+1} \qquad (3.51) \\ &= \sigma^2(m) + \frac{(x_{m+1} - X_1(m))(x_{m+1} - X_1(m+1)) - \sigma^2(m)}{m+1}, \qquad (3.52)\end{aligned}$$

which is perfect to the calculations in the computer. Beyond that, as we will see in section 3.3.4, this expression can be used to measure the estimator from the values of the variance inside a block of measurements.

3.3.3 Kurtosis

The kurtosis, k, is a measure of the deviation of a distribution relatively to a Gaussian distribution (in which $k = 0$), where the fourth order moments are relevant. The standard expression, for an Ising model in zero magnetic field, is:

$$k = \frac{\left\langle (x - \langle x \rangle)^4 \right\rangle}{\left\langle (x - \langle x \rangle)^2 \right\rangle^2} - 3. \qquad (3.53)$$

In phase transitions, it is related with the Binder's cumulant of the order parameter,

$$U_B = -\frac{k}{3}. \qquad (3.54)$$

The Binder's cumulant is, frequently, used to measure T_c. When one plots the Binder's cumulant as function of temperature, for several system sizes, and for a given dimensionality, the curves intersect precisely in the critical temperature [3].

3.3.3.1 Recursion relations for kurtosis

As in previous cases, it is possible to write a kurtosis recurrence relation to avoid the numerical convergence problems. Thus, numerical evaluation of the kurtosis is significantly improved.

The easiest way to write the recurrence relation is to exploit the central moments, R_r. By definition,

the r^{th} central moment normalized by the size of the system is given by:

$$R_r\left(L\right) = \frac{1}{L}\sum_{i=0}^{L-1}\left(x_i - X_1(L)\right)^r. \tag{3.55}$$

Looking this way, expression (3.53) can be rewritten as:

$$k\left(m+1\right) = \frac{R_4\left(m+1\right)}{R_2^2\left(m+1\right)} - 3. \tag{3.56}$$

The most important central moments for our calculation of the recurrence relation are:

$$R_1\left(m+1\right) = 0; \tag{3.57}$$

$$R_2\left(m+1\right) = X_2\left(m+1\right) - X_1^2\left(m+1\right); \tag{3.58}$$

$$R_3\left(m+1\right) = X_3\left(m+1\right) - 3X_2\left(m+1\right)X_1\left(m+1\right) + 2X_1^2\left(m+1\right); \tag{3.59}$$

$$R_4\left(m+1\right) = X_4\left(m+1\right) - 4X_3\left(m+1\right)X_1\left(m+1\right) + 6X_2\left(m+1\right)X_1^2\left(m+1\right) + 5X_1^4\left(m+1\right). \tag{3.60}$$

We can write $R_4\left(m+1\right)$ and $R_3\left(m+1\right)$ at the expense of the other central moments, always thinking about avoiding numerical convergence problems. Note that R_2 is the estimator for variance, in the limit of large m. Doing the math, we obtain:

$$\begin{aligned} R_2\left(m+1\right) &= \frac{1}{m+1}\sum_{i=1}^{m+1}\left(x_i - X_1\left(m+1\right)\right)^2 \\ &= \frac{m}{m+1}R_2(m) + \frac{m}{\left(m+1\right)^2}\left(x_{m+1} - X_1\left(m\right)\right)^2, \end{aligned} \tag{3.61}$$

for $R_3\left(m+1\right)$:

$$\begin{aligned} R_3(m+1) &= \frac{1}{m+1}\sum_{i=1}^{m+1}\left(x_i - X_1(m+1)\right)^3 \\ &= \frac{m}{m+1}R_3(m) - 3\frac{m}{(m+1)^2}R_2(m)\left(x_{m+1} - X_1(m)\right) \\ &+ \frac{m(m-1)}{(m+1)^3}\left(x_{m+1} - X_1(m)\right)^3, \end{aligned} \tag{3.62}$$

and for $R_4(m+1)$:

$$\begin{aligned} R_4(m+1) &= \frac{1}{m+1}\sum_{i=1}^{m+1}\left(x_i - X_1(m+1)\right)^4 \\ &= \frac{m}{m+1}R_4(m) - 4R_3(m)\left(x_{m+1} - X_1(m)\right)\frac{m}{(m+1)^2} \\ &+ 6R_2(m)\left(x_{m+1} - X_1(m)\right)^2\frac{m}{(m+1)^3} \\ &+ \left(x_{m+1} - X_1(m)\right)^4\frac{m\left((m+1)^2 - 3m\right)}{(m+1)^4}. \end{aligned} \tag{3.63}$$

Using a box with $L = 100$ and $p = 0.3$, we calculated the distribution of the Binder's cumulant, for different m. One verifies that, as one increases the number of points, the values for the Binder's cumulant get closer to the real value (fig. (3.7)). The analytic value for the Binder's cumulant was found appealing to (3.53), and it is:

$$Binder's\ cumulant = \frac{1}{3}\left(3 - \frac{3\left(-7 - 7L + 3L^2 + 3L^3\right)}{5(L-1)(L+1)^2}\right). \tag{3.64}$$

In the plot of the figure (3.7), "Exact Binder" refers to the value for (3.64), when $L = 100$.

3.3.4 Blocks' method

So far, we studied methods for the calculation of estimator's errors and more efficient methods for computational implementation of the mean value, variance and kurtosis. However, we can not forget that there are still correlations between the data, that can introduce some errors in the estimation of the values. In this subsection, we will study a strategy to overcome this problem.

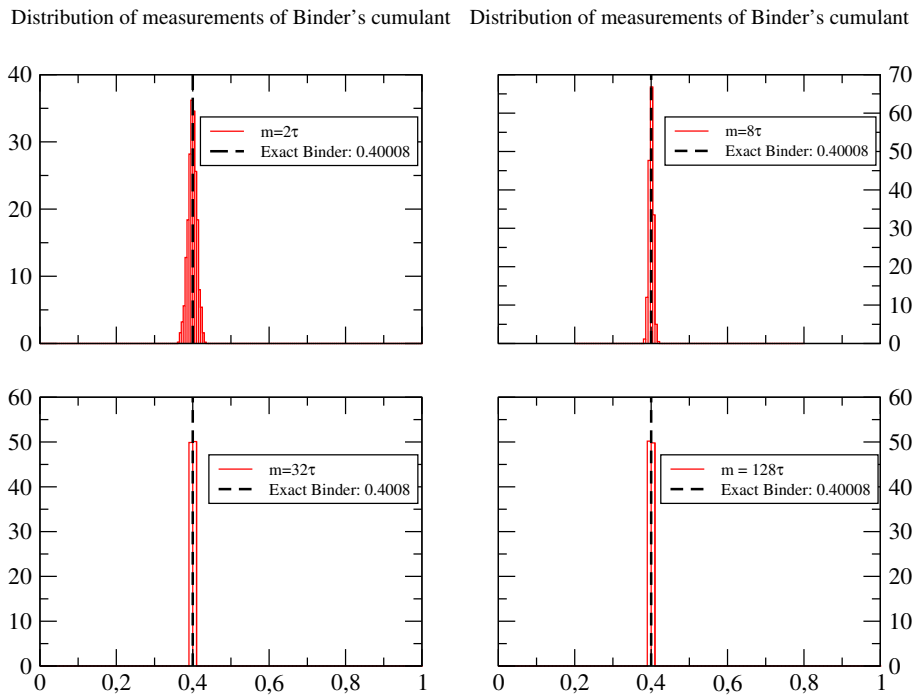

Figure 3.7: Using different number of points (m), proportional to τ , we get the distribution of measurements of $k\,(m)$. The data was obtained using a box of length $L = 100$ and $p = 0.3$.

Thus, we will use a block based method. It consists in split the data into blocks almost uncorrelated. The correlation time between consecutive blocks become the correlation time of the states in the borders of the blocks. When we choose a block size of several correlation times, we are decreasing significantly the correlation between consecutive average values.

3.3.4.1 Correlation between blocks

We are interested in the study of some variable x , so that the sequence of states in time correspond to a sequence of values x_t with $t = 1, \cdots, N$. For commodity, we will organize the data in a sequence of N_b blocks:

$$\underbrace{x_{11}, \cdots, x_{1m}}_{1st\ block}, \underbrace{x_{21}, \cdots, x_{2m}}_{2nd\ block}, \cdots, \underbrace{x_{N_b 1}, \cdots, x_{N_b m}}_{N_b th\ block}. \tag{3.65}$$

To consolidate the argument, we will estimate the correlation of some mean value between consecutive blocks. Let us consider the mean values:

$$\begin{aligned} B_1(m) &= \frac{1}{m}\sum_{i=1}^{m} x_i, \\ B_2(m) &= \frac{1}{m}\sum_{i=m+1}^{2m} x_i, \end{aligned} \tag{3.66}$$

in which B_1 is the estimator for the mean value for the first block, and B_2 is the estimator for the mean value for the immediately following block. The correlation between the two mean values is given by

$$C_b = \frac{\langle B_1 B_2\rangle - \langle B_1\rangle\langle B_2\rangle}{\sqrt{\langle B_1^2\rangle - \langle B_1\rangle^2}\sqrt{\langle B_2^2\rangle - \langle B_2\rangle^2}} = \frac{\langle B_1 B_2\rangle - \langle x\rangle^2}{\sqrt{\langle B_1^2\rangle - \langle x\rangle^2}\sqrt{\langle B_2^2\rangle - \langle x\rangle^2}}. \tag{3.67}$$

Studying the averages inside the same block, we get:

$$\begin{aligned} \langle B_1^2\rangle - \langle B_1\rangle^2 &= \frac{\chi_{xx}}{m^2}\sum_{i=1}^{m}\sum_{j=1}^{m} C_{xx}(i-j) \\ &\approx \chi_{xx}\frac{1+2\tau(x,x)}{m}, \end{aligned} \tag{3.68}$$

and, the cross average over the two blocks,

$$\begin{aligned} \langle B_1 B_2\rangle - \langle x\rangle^2 &= \frac{\chi_{xx}}{m^2}\sum_{i=1}^{m}\sum_{j=m+1}^{2m} C_{xx}(i-j) \\ &= \frac{\chi_{xx}}{m^2}\sum_{i=1}^{m}\sum_{j=1}^{m} C_{xx}(i-j+m) \\ &\approx \frac{\chi_{xx}}{m^2}\sum_{i=1}^{\infty} i\, C_{xx}(i) \qquad (3.69) \\ &\sim \chi_{xx}\frac{\tau^2}{m^2} \qquad (3.70) \end{aligned}$$

where in (3.69) we assumed that $\tau \ll m$ and in (3.70) we assumed that the correlation is an exponential function. The correlation between consecutive blocks becomes:

$$C_b = \frac{m}{1+2\tau}\frac{\tau^2}{m^2} \approx \frac{\tau}{2m}, \tag{3.71}$$

where we assumed that $1 \ll \tau \ll m$. These results justify the use of the dispersion of the mean value of the blocks to estimate the error.

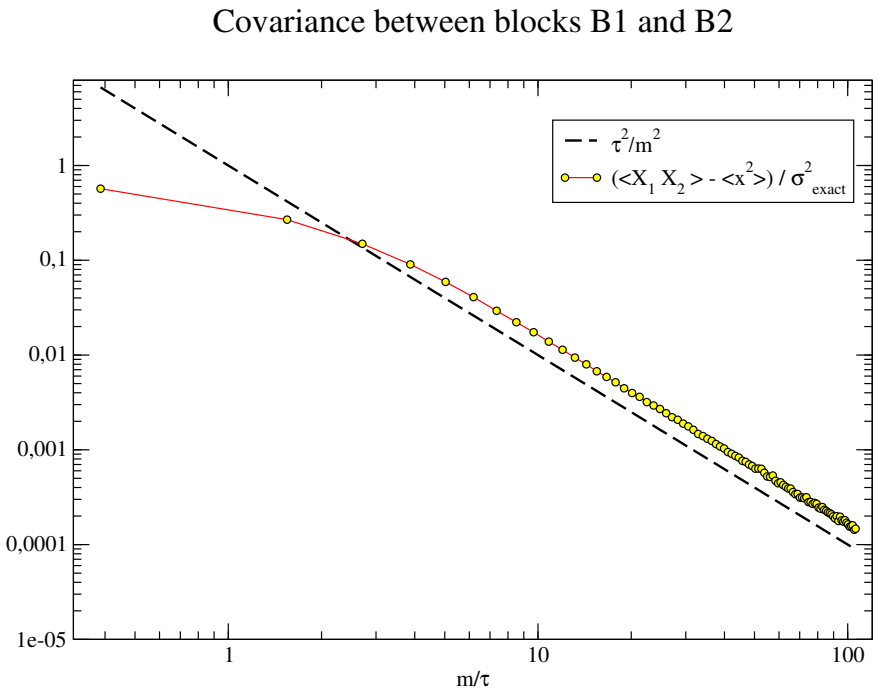

Figure 3.8: The covariance between blocks B_1 and B_2, and the comparison with the right-hand side of (3.70), using a box of $L = 100$ and $p = 0.3$.

We plot, in fig. (3.8), the covariance between two consecutive blocks as function of $\frac{\tau^2}{m^2}$. We can check that the covariance between two consecutive blocks goes with $\frac{\tau^2}{m^2}$, as predicted by (3.70).

3.3.4.2 Estimators for the system divided in blocks

We have the data divided in blocks of size m. So far, we presented the estimators for the mean value, variance and kurtosis inside the block level. Now, the task is to find the best estimators for these quantities, combining the data from the different blocks, in order to get the overall estimators. We achieve estimators that are a generalization of (3.38) (mean value), (3.48) (variance) and (3.56) (kurtosis) for the whole system:

$$\begin{aligned} E_T(x^n) &= X_n(T) \\ E_T(\sigma^2) &= T\frac{X_2(T) - X_1^2(T)}{T - 2\tau_{xx} - 1} \\ E_T(k) &= \frac{R_4(T)}{R_2^2(T)} - 3, \end{aligned} \tag{3.72}$$

where $T = m\,N_b$ is the total number of collected data. We should notice that we need to evaluate an estimation of the value of the autocorrelation time to correct the estimator of variance.

3.3.4.3 Recursion relations over blocks

Once again, until now, we just have the recursion relations to be implemented inside the block. Nevertheless, to obtain the overall estimators, for the system, we need to combine the different statistical measures from different blocks. We will present the recursion relations for the set of equations (3.72). Let us define the estimator of the mean value, variance and kurtosis up to the $l-th$ block:

$$\begin{aligned} Z_1(l) &= X_1(ml) \\ S_\alpha(l) &= R_\alpha(ml) \\ K(l) &= \frac{S_4(ml)}{S_2^2(ml)} - 3 \end{aligned} \tag{3.73}$$

For the mean value, the recursion relation is straightforward:

$$Z_1(l+1) = Z_1(l) + \frac{z_{l+1} - Z_1(l)}{l+1}, \tag{3.74}$$

because the size of each block is constant. Here, z_{l+1} stands for the mean value of block $l+1$, i.e:

$$z_{l+1} = \frac{1}{m+1} \sum_{i=ml+1}^{m(l+1)} x_i \tag{3.75}$$

For the variance and kurtosis, it is not so direct as the mean value. The recursion relations are [6]:

- for the variance:

$$S_2(l+1) = S_2(l) + \frac{1}{l+1}\left(s_2(l) - S_2(l)\right) + \frac{l}{(l+1)^2}\left(Z_1(l+1) - z_{l+1}\right)^2; \tag{3.76}$$

- for the 3^{rd} moment:

$$\begin{aligned} S_3(l+1) &= S_3(l) + \frac{1}{l+1}\left(s_3(l) - S_3(l)\right) \\ &+ \frac{\left(Z_1(l+1) - z_{l+1}\right)^3}{(l+1)^3} l(l+1) \\ &+ \frac{3\left(Z_1(l+1) - z_{l+1}\right) l}{(l+1)^2}\left(s_2(l) - S_2(l)\right); \end{aligned} \tag{3.77}$$

- for the 4^{th}moment:

$$\begin{aligned} S_4(l+1) &= S_4(l) + \frac{1}{l+1}\left(s_4(l) - S_4(l)\right) \\ &+ \left(Z_1(l+1) - z_{l+1}\right)^4 \frac{l^3 - l^2 + l}{(l+1)^4} \\ &+ 6\left(Z_1(l+1) - z_{l+1}\right)^2 \frac{\left(l^2 s_2(l) + l\, S_2(l)\right)}{(l+1)^3} \\ &+ \frac{4\left(Z_1(l+1) - z_{l+1}\right) l}{(l+1)^2}\left(s_3(l) - S_3(l)\right), \end{aligned} \tag{3.78}$$

in which $s_\alpha(l)$ is the central moment of the block l:

$$s_\alpha(l) = \frac{1}{m}\sum_{i=ml+1}^{m(l+1)} \left(x_i - z_l\right)^\alpha \tag{3.79}$$

The computational program is more efficient when we use these recursion relations. Therefore, the obtained data is more accurate. Nevertheless, we should remark that, even using all these methods - to split into blocks, to use the recursion relations - it is necessary to take much longer so that we can have statistic enough.

3.3.4.4 Error bar

The error bars are obtained from estimator for variance of a quantity, assuming that the correlation between blocks is very small. In fact, it is possible to find some correlations between consecutive blocks, in the edges. However, this is a small effect.

We calculate the estimator for the mean value of position, its variance and kurtosis of each block:

$$\bar{Q} = \frac{1}{l}\sum_{i=1}^{l} Q_i, \tag{3.80}$$

in which Q refers to the mean value, variance or kurtosis of each block. Thus, the squared error is given by:

$$\begin{aligned} \triangle^2 \bar{Q} &= \frac{\sigma_Q^2}{l} \\ &= \frac{1}{l}\left(\overline{Q^2} - \bar{Q}^2\right)\frac{l}{l-1} \\ &= \left(\overline{Q^2} - \bar{Q}^2\right)\frac{1}{l-1} \end{aligned} \tag{3.81}$$

If the blocks are very large, the correlations between points inside the block are small and the error

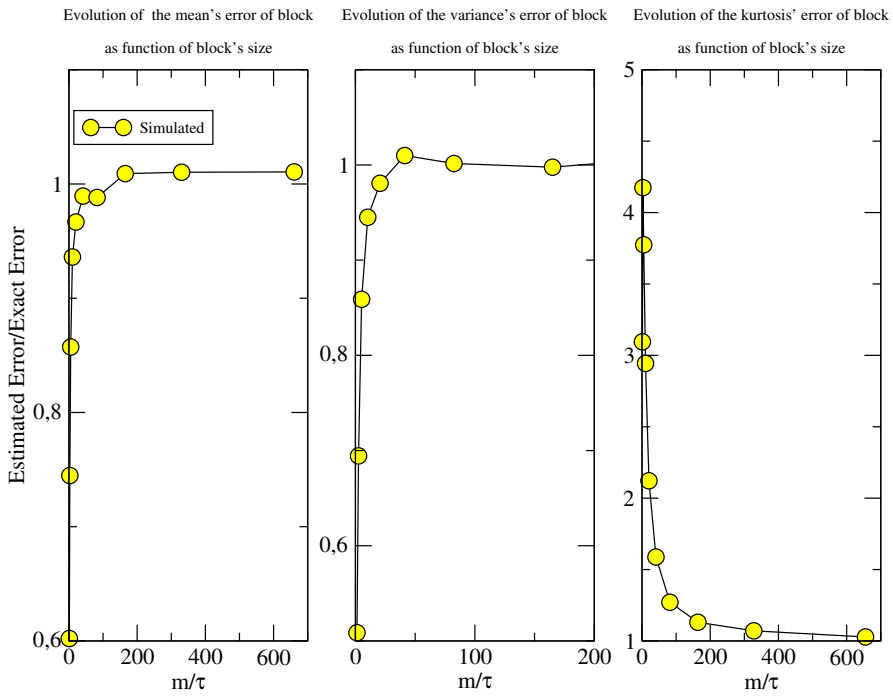

Figure 3.9: Evolution of block's errors.

estimate is better. We can illustrate this in the following way: we simulated a large block ("an infinite block") and calculated its mean's error, variance's error and kurtosis' error. This quantity is our exact error of the block for its mean, variance and kurtosis. Then, we generated smaller blocks of size m and we did the same calculations. We plotted the ratio between estimated error (it is the error from smaller blocks) and the exact error and we get the fig. (3.9). As we can see in plot (3.9), the larger the block size, the more accurate error we get.

3.4 Final considerations of the chapter

The results of this chapter are implemented in a computational program. Using the program, it is possible to study the critical region of 2D and 3D Ising model, which is one of the aims of this proposal. The analysis of phase transition for those systems will be performed in the next chapter.

Chapter 4

Analysis of 2D and 3D Ising Model phase transition from numerical methods

4.1 Thermodynamic functions of 2D and 3D Ising Model

In this section, we will see and discuss what happens to the thermodynamic functions for 2D and 3D Ising Model. The β_c for 2D is known exactly (it is the inverse of (1.8)) . However, we only have estimates for the same quantity in 3D: $\beta_{c\,3D} = 0.2216595 \pm 0.0000026$ [11]. We will show some numerical results that allow us to find the β_c.

In plot (4.1), we see the plots for 2D Ising Model. We used the technique of splitting the data in blocks to get accurate values. Besides, we represent all the thermodynamic functions with the estimated error bar, as was explained in chapter 3. It is interesting to notice that, for specific heat and magnetic susceptibility, as we get closer β_c, the function has a peak, instead of diverging. It is an expected result, since we are dealing with finite systems. The peak reaches high values for larger systems.

In fig. (4.2) we plot the Binder's cumulant. The Binder's cumulant was introduced in the subsection 3.3.3. It is useful for determining the critical temperature, once that the curves of Binder's cumulant will intersect exactly in the critical temperature. This is what we see in the right-hand side of the plot (4.2). We observe also that the smallest system (lattice with 8^2 spins) does not intersect in the same point of other systems; once again, it occurs because we are dealing with finite systems. So, numerically, from the graph (4.2), we can say that β_c is in the range $[0.440, 0.441]$, that agrees with the exact value: $\beta_c = \frac{1}{\frac{2}{\ln(1+\sqrt{2})}} \cong 0.44068679351$.

For 3D Ising model, we studied 3D simple-cubic Ising model. The plots obtained are in fig. (4.3). The plots (fig. (4.3)) for 3D model are similar to 2D case, except the critical temperature. The specific heat and the magnetic susceptibility show a peak near the critical temperature, instead of diverging. Again, for larger systems, the peak reaches higher values. We show plots only for three lattice sizes,

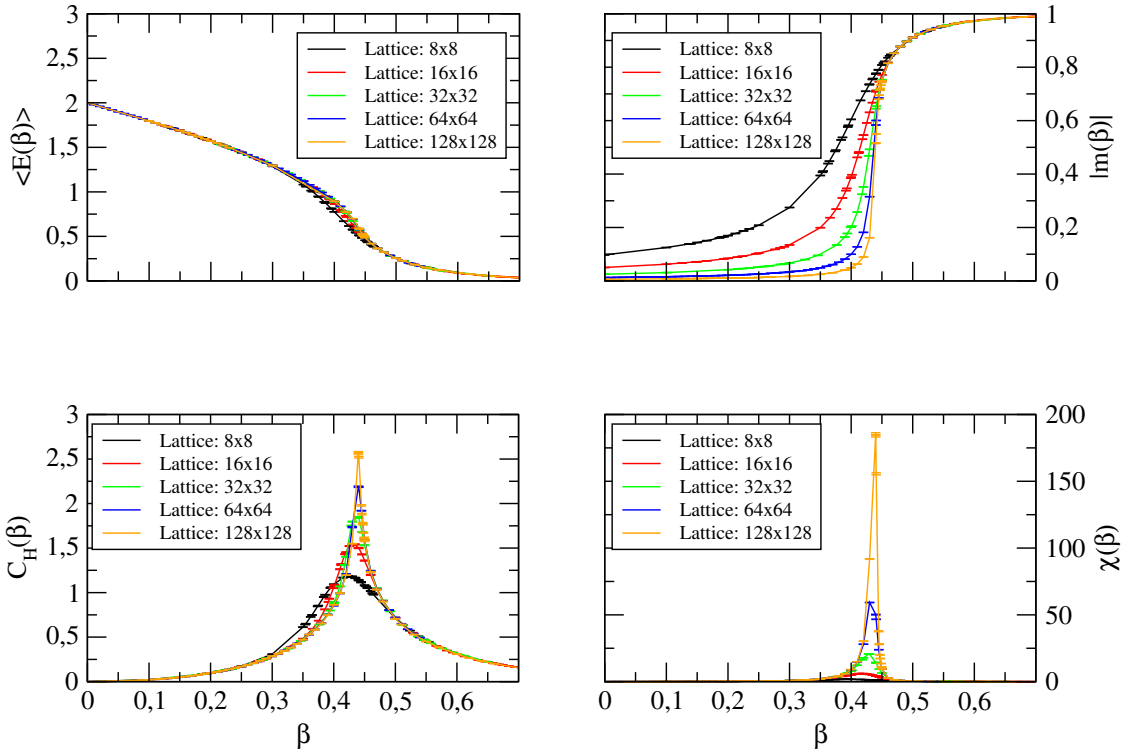

Figure 4.1: Plots of energy, absolute magnetization, specific heat and susceptibility as function of β for 2D Ising Model, using Monte Carlo Methods.

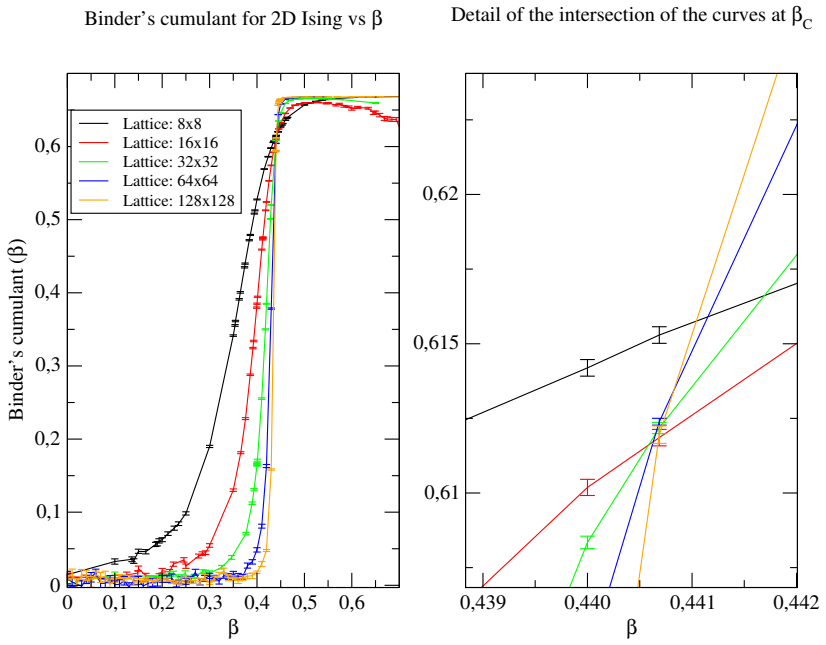

Figure 4.2: The Binder's cumulant as function of β for 2D Ising model, using Monte Carlo Methods.

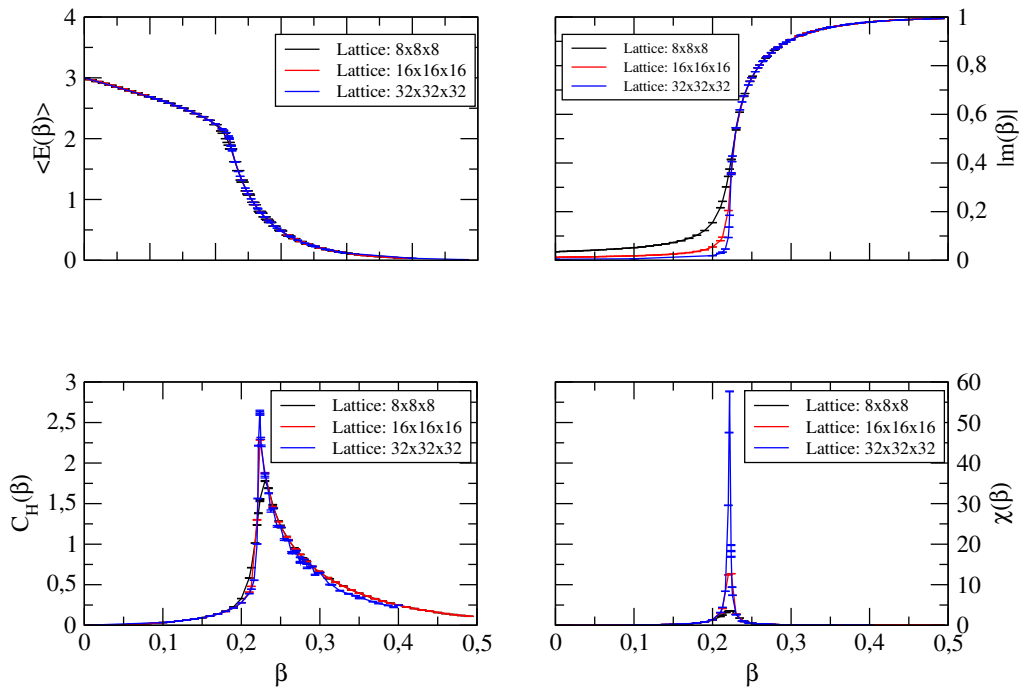

Figure 4.3: Plots of energy, absolute magnetization, specific heat and susceptibility as function of β for 3D Ising Model, using Monte Carlo Methods.

d	2	3
α	0	$0.110(1)$
β	$\frac{1}{8}$	$0.3265(3)$
γ	$\frac{7}{4}$	$1.2372(5)$
ν	1	$0.6301(4)$

Table 4.1: Critical exponents for 2D and 3D Ising Model. d denotes dimensionality. From: [12], [18].

because it takes longer to have accurate results for large lattices.

The Binder's cumulant plot for 3D Ising model is in the fig.(4.4). In fig. (4.4), we used also a function with a lattice of 64^3 spins. However, this function has few points, and it takes longer to get a value for $\beta > \beta_c$. According to the right-hand side of the plot (4.4), β_c is in the range $[0.220, 0.222]$. It is consistent with estimates [11] for this β_c.

These plots give us a general vision of the thermodynamic functions; however, we want to study the critical region. Namely, we want to get the critical exponents. The critical exponents for 2D Ising Model and for 3D Ising Model are in table (1.1).

Notice that the exponents for 2D Ising Model are exact, while the critical exponents of 3D are recent estimates [12]. In the next section, we will use finite size scaling to find the values of critical exponents.

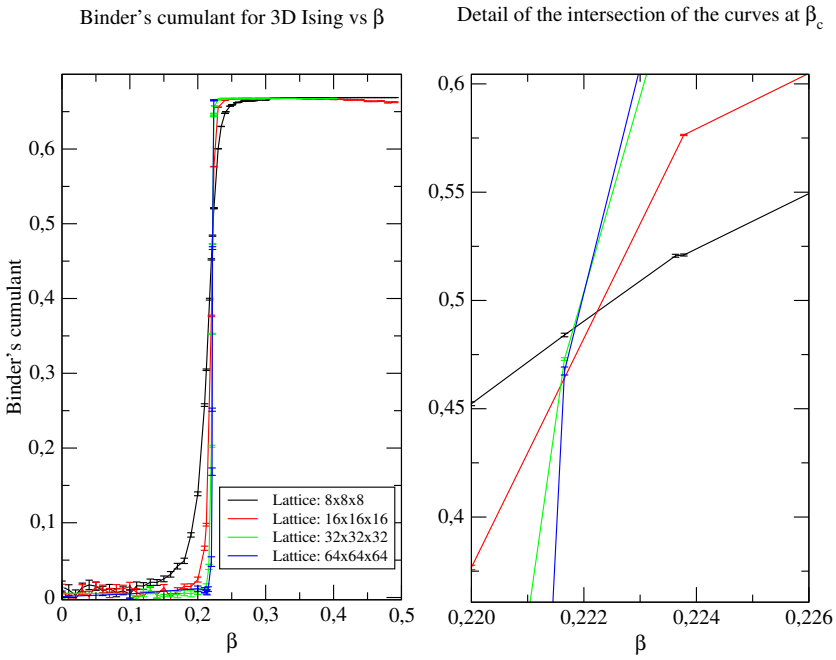

Figure 4.4: The Binder's cumulant as function of β for 3D Ising model, using Monte Carlo Methods.

4.2 The Finite Size Scaling

As refered in the section 1.3, a finite system does not have a phase transition. This is easy to understand from the partition function since it is a sum over finite number of regular functions, i.e., $e^{-\beta E_\mu}$. The fact that there is no phase transition can also be understood from the definition of correlation length ξ. It defines a region of length ξ where the points are correlated. Since the system is finite, the correlation length is also restricted to be finite. However, these effects are important only near the critical point. We know that the correlation length becomes small when it is not near T_c. Thus, the interactions of the degrees of freedom in this regime do not feel the finite length of the system; they behave as if the system is infinite. Recall that Monte Carlo methods are applied to finite systems, so we need to introduce a method to extract information from the critical region, knowing that the system has a finite length. For this purpose, we introduce a method called finite size scaling (FSS), that allows to extract the critical data from a finite system by studying how the physical observables vary with the length scale L.

The idea behind this method was already used on the second chapter, where we had to determine the dynamic exponent z, that controls how the autocorrelation time, τ, scales with the system size, at the critical temperature. In this section, we will study how the magnetization, magnetic susceptibility and specific heat go with temperature, for various system sizes. As was remarked, at the off-criticality the degrees of freedom behave as if they were in infinite system. The differences will only appear near the

critical point. Thus, the FSS will depend on how accurately the critical temperature is known. It is not our aim obtain a sensible measure for the error made in the estimation of the critical exponents using FSS.

Let us give an example of FSS by studying the magnetic susceptibility. The magnetic susceptibility measures how the magnetization changes when there is an infinitesimal increment in the magnetic field, h. In the present study, we restrict $h = 0$. Near the critical point, in a system with zero magnetic field, the magnetic susceptibility behaves as

$$\chi \sim |t|^{-\gamma} . \tag{4.1}$$

FSS studies how the system changes with the system size. Thus, we should now try to rephrase (4.1) in terms of a length scale, preferably ξ. For this purpose, note that the correlation length behaves as

$$\xi \sim |t|^{-\nu} . \tag{4.2}$$

Therefore, the magnetic susceptibility can be written in terms of the correlation length as

$$\chi \sim \xi^{\frac{\gamma}{\nu}}. \tag{4.3}$$

According to what was explained above, this should depend also on the system size or, in other words,

$$\chi = \xi^{\frac{\gamma}{\nu}} \chi_0 \left(\frac{L}{\xi} \right), \tag{4.4}$$

where χ_0 is a dimensionless function, satisfying

$$\chi_0(x) = \begin{cases} const, & x \gg 1 \\ 0, & x \to 0. \end{cases} \tag{4.5}$$

It is more convenient to express this relation in terms of the reduced temperature, instead of the correlation length ξ . This can be done by introducing another function $\tilde{\chi}$ that is related to χ_0 by

$$\tilde{\chi}\left(x\right) = x^{-\gamma} \chi_0 \left(x^{\nu}\right). \tag{4.6}$$

Thus, the susceptibility can be written as

$$\chi = L^{\frac{\gamma}{\nu}} \tilde{\chi} \left(L^{\frac{1}{\nu}} t \right). \tag{4.7}$$

Notice that, in a Monte Carlo simulation, we measure the function χ. This should be done for several sizes of the system and for values of the temperature close to the critical point. An important remark is that $\tilde{\chi}\left(x\right)$ does not depend on L, so this relation shows that there is a set of exponents γ and ν

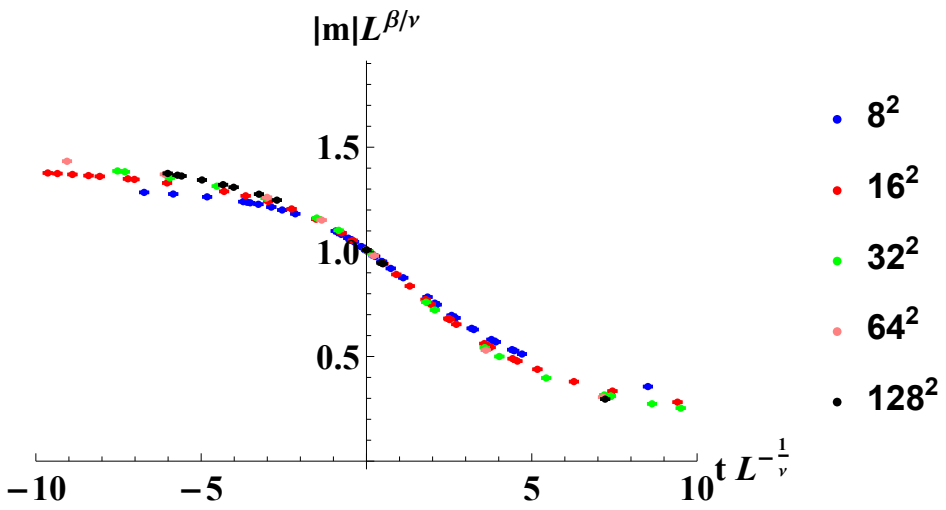

Figure 4.5: FSS for absolute magnetization for 2D Ising Model. t, in the x-axis, denotes reduced temperature.

that allow to collapse all data points from several system sizes to one curve. This can be done in the following way: rescale χ by $L^{\frac{\nu}{\gamma}}$ and express it in terms of the rescaled temperature $L^{\frac{1}{\nu}}t$; then, we should observe that the plot $\chi L^{\frac{\nu}{\gamma}}$ in terms of $tL^{\frac{1}{\nu}}$ reduces to a single curve for all points with different L. Note that the reduced temperature t is not known for every model. Nevertheless, we can get an estimate for it by searching the temperature in which the susceptibility achieves it maximum.

The FSS can be applied also to the specific heat and magnetization, using an argument similar to the described above. The FSS for that quantities give the following expressions:

$$c = L^{\frac{\alpha}{\nu}}\tilde{c}\left(L^{\frac{1}{\nu}}t\right) \tag{4.8}$$

$$m = L^{-\frac{\beta}{\nu}}\tilde{m}\left(L^{\frac{1}{\nu}}t\right) \tag{4.9}$$

The data obtained from Monte Carlo simulations can also be collapsed into one curve, using the functional dependence of the previous equations. Using Monte Carlo data, varying the value of the critical exponents until we see the collapse of the curves, we obtained the following results:

- 2D Ising Model:
  - Absolute magnetization:

The exponents involved in the FSS for the absolute magnetization are β and ν. The collapse in fig. (4.5) was obtained with $\beta = 0.125$ and $\nu = 1$. These results for critical exponents agree with

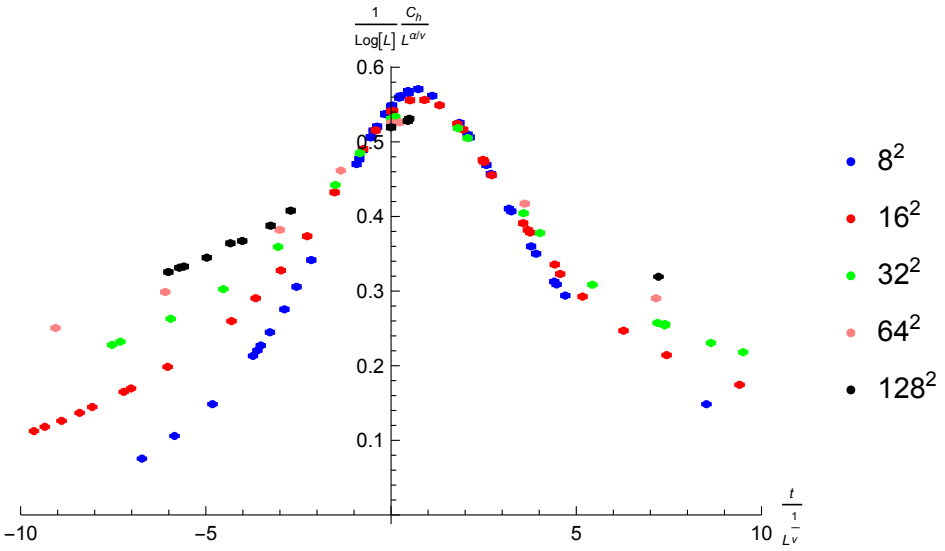

Figure 4.6: FSS for specific heat for 2D Ising Model. t, in the x-axis, denotes reduced temperature.

values in the table (4.1). Notice that the collapse is better at $t = 0$, that corresponds to the critical temperature, as expected.

- Specific heat:

The exponents involved in the FSS for the specific heat are α and ν. In the plot (4.6) the values used were: $\alpha = 0$ and $\nu = 1$. Remark that the specific heat has a logarithmic divergence; in order to get the collapse of the curves, it was necessary to divide the left-hand side of (4.8) by $\log(L)$.

- Magnetic Susceptibility:

The exponents involved in the FSS for the susceptibility are γ and ν. The collapse in fig. (4.7) was obtained with $\gamma = 1.75$ and $\nu = 1$. These results for critical exponents agree with values in the table (4.1). Once again, the collapse is better at $t = 0$, as expected.

- 3D Ising Model:

For the case of 3D Ising Model, it is more difficult to have accurate values for the thermodynamic functions. In spite of using the blocks' method and the recursion relations in the computational program, to turn the data more accurate and the program more efficient, it takes longer to get the accurate values, for a 3D lattice. The larger is the size of the lattice, the longer it takes to get results. For this reason, we present the results for only three lattices.

- Absolute magnetization:

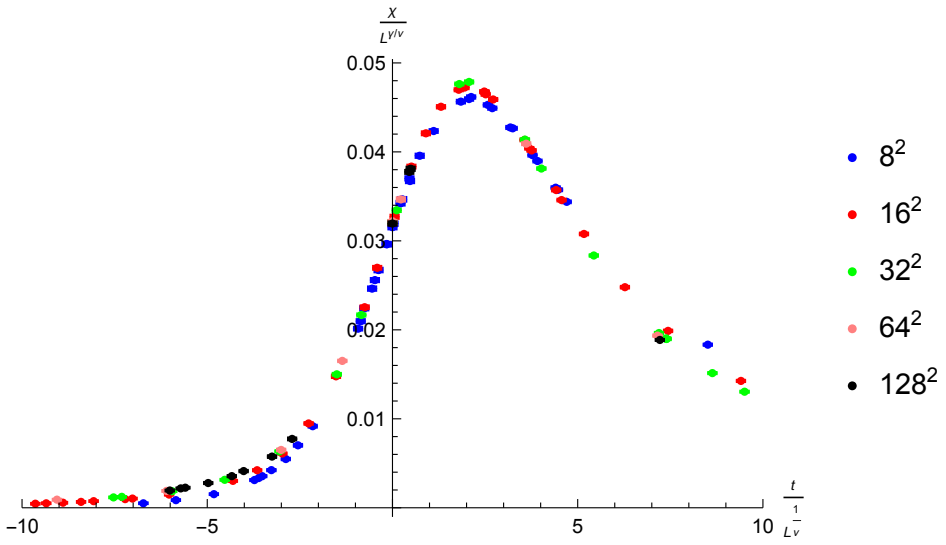

Figure 4.7: FSS for susceptibility, for 2D Ising Model. t, in the x-axis, denotes reduced temperature.

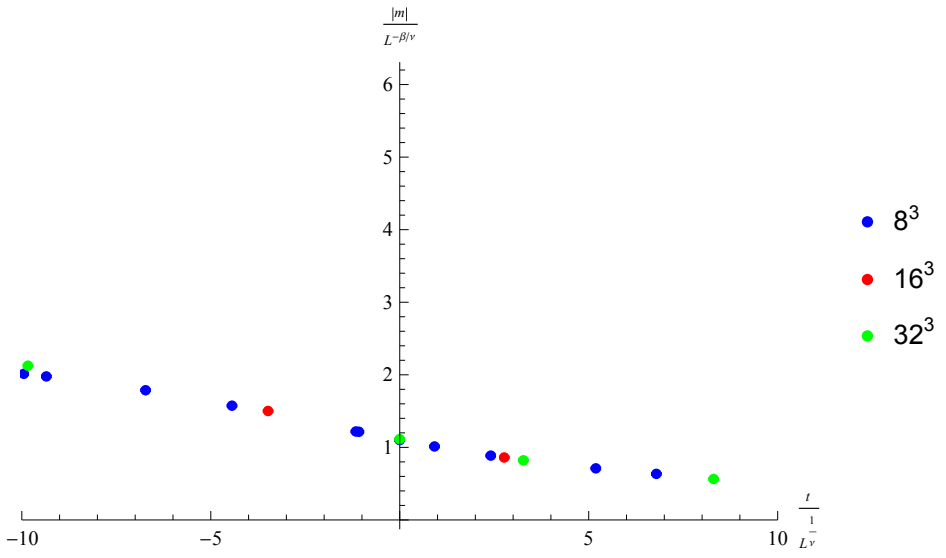

Figure 4.8: FSS for absolute magnetization, for 3D Ising Model. t, in the x-axis, denotes reduced temperature.

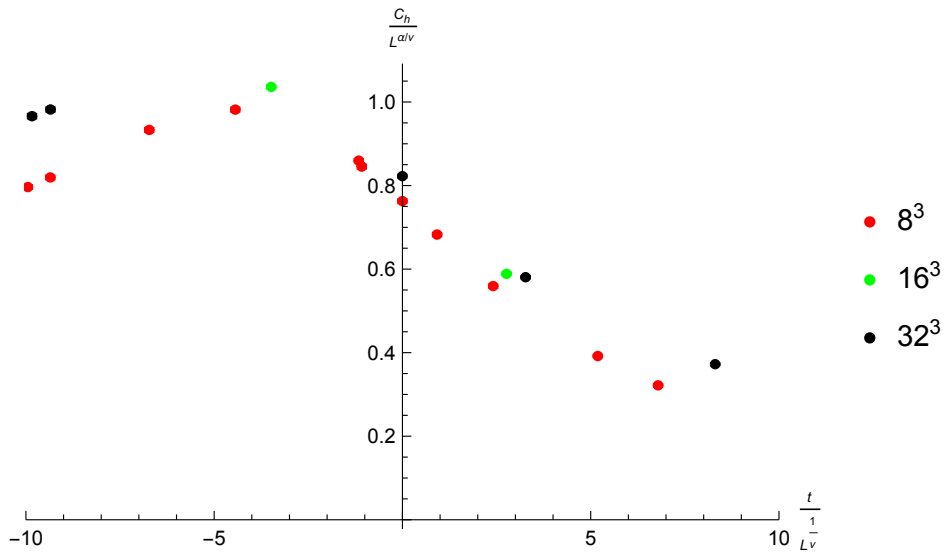

Figure 4.9: FSS for specific heat for 3D Ising Model. t, in the x-axis, denotes reduced temperature.

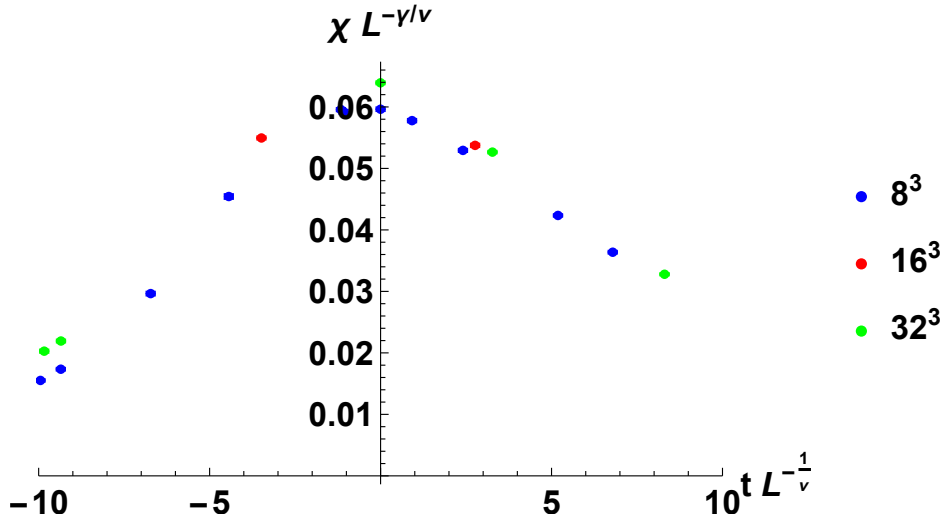

Figure 4.10: FSS for susceptibility for 3D Ising Model. t, in the x-axis, denotes reduced temperature.

The collapse in fig. (4.8) was obtained with $\beta = 0.3265$ and $\nu = 0.6301$. These results for critical exponents agree with values in the table (4.1).

– Specific heat:

The values used in fig.(4.9) were $\alpha = 0.18$ and $\nu = 0.6301$. Notice that, in 3D Ising Model, the divergence of the specific heat is not logarithmic - α is nonzero.

– Magnetic Susceptibility:

The best collapse, that is presented in fig. (4.10), was obtained with $\gamma = 1.2372$ and $\nu = 0.6301$. These results for critical exponents agree with values in the table (4.1).

Chapter 5

Surface critical behavior results

In this section we will present the results obtained from Monte Carlo simulations for the three dimensional Ising model in the presence of a spherical boundary. The procedure to simulate the Ising model in the presence of a spherical boundary is the following: we considered a three dimensional lattice with spins at each lattice points, drew an imaginary sphere with a certain radius in this lattice and, then, we neglected all spins that stayed outside this region. In fig. (5.1) we give an example of this for a two dimensional lattice.

As explained in the introduction (see subsection 1.8.5), the one and two point function of local operators in the presence of a spherical boundary contain specific characteristics of conformal invariance. We will be interested in the long wave length physics of the system, where it can be effectively viewed as a continuum theory with local operators. The simplest local lattice operator that is invariant under the lattice symmetries, that preserve the point x and is odd under spin-flip is the local spin field $s\left(x\right)$. In the sector of the operators invariant under the spin-flip and the lattice symmetries, the simplest operators are the identity I and the energy density:

$$e\left(x\right)=\frac{1}{6}\sum_{\delta}s\left(x\right)s\left(x+\delta\right), \tag{5.1}$$

where $x+\delta$ runs over the 6 nearest neighbors of x. The map between the lattice fields to the local operators in the 3D Ising model assumes the following form,

$$\begin{aligned} s\left(x\right) &= b_{s\sigma}a^{\Delta_{\sigma}}\sigma\left(x\right)+b_{s\sigma'}a^{\Delta_{\sigma'}}\sigma'\left(x\right)+\ldots \\ e\left(x\right) &= b_{eI}I\left(x\right)+b_{e\epsilon}a^{\Delta_{\epsilon}}\epsilon\left(x\right)+b_{e\epsilon'}a^{\Delta_{\epsilon'}}\epsilon'\left(x\right)+\ldots, \end{aligned} \tag{5.2}$$

where a is the lattice spacing, $\Delta_{\mathcal{O}}$ is the conformal dimension of the operator. We have organized the

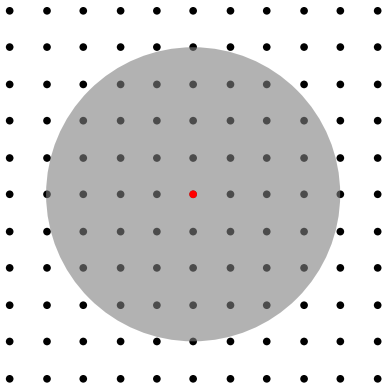

Figure 5.1: In this example we consider a two dimensional lattice with eleven points in each side. Then, we consider a circle with radius of four lattice spacings. We count only the spins that stay inside the disk.

local operators according to their dimension or, in other words $\Delta_\sigma < \Delta_{\sigma'}$ and $\Delta_\epsilon < \Delta_{\epsilon'}$ (notice that $I(x)$ is the identity operator, with $\Delta_I = 0$, and there is no field with dimension smaller than it). For the 3D Ising model, the best estimates for these dimensions are [9], [10] :

$$\Delta_\sigma \approx 0.51815, \quad \Delta_{\sigma'} \approx 4.5, \quad \Delta_\epsilon \approx 1.4126, \quad \Delta_{\epsilon'} \approx 3.83, \tag{5.3}$$

which can be compared with the two dimensional results which are known exactly,

$$\Delta_\sigma = \frac{1}{8}, \quad \Delta_{\sigma'} = \frac{33}{8}, \quad \Delta_\epsilon = 1, \quad \Delta_{\epsilon'} = 4. \tag{5.4}$$

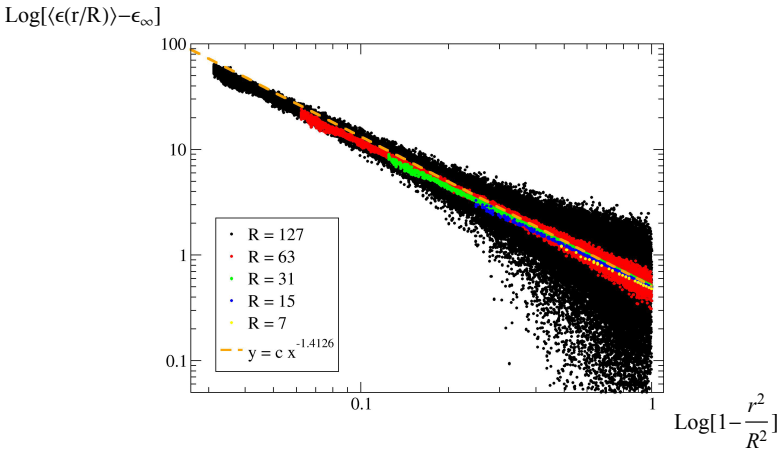

Figure 5.2: One point function of the operator $\epsilon(x)$ in the presence of a spherical boundary.

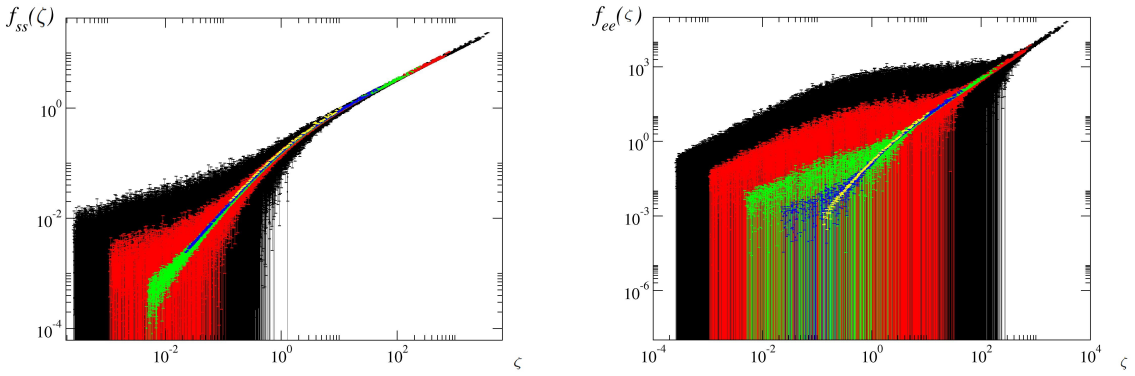

(a) Two point function of the local operator $\sigma\left(x\right)$.

(b) Two point function of the local operator $\epsilon\left(x\right)$.

Figure 5.3: Two point function of the local operators.

The simplest one point function that is possible to compute is the local energy density $\epsilon\left(x\right)$, since the one point function of the field $\sigma\left(x\right)$ is zero. In fig. (5.2), we present the results for the one point function of ϵ,

Notice that, for all different system sizes, the one point function of the operator $\epsilon\left(x\right)$ satisfies the functional form predicted by conformal invariance. Recall that, in this case, the prediction was that the one point function should go as a simple power law of $\left(1-\left(\frac{\vec{r}}{R}\right)^{2}\right)$, as stated in (1.85). Moreover, the exponent of the one point function is precisely the dimension of the operator ϵ. The conformal bootstrap gives one of the most precise measurements of this exponent: $\Delta_{\epsilon}=1.41267$. In fig.(5.2) we have plotted this and it clearly agrees with the data. Let us point out that the dispersion of the points for the system with size $R=127$ is large because the lack of statistics.

For the case of the two point function in the presence of a boundary, we will use both $\sigma\left(x\right)$ and also $\epsilon\left(x\right)$. As emphasized in the introduction, we expect that the two point function should depend just on a non-trivial function of the conformal cross ratio ζ,

$$\left\langle \mathcal{O}_{\Delta}\left(\vec{r}_{1}\right)\mathcal{O}_{\Delta}\left(\vec{r}_{2}\right)\right\rangle =\frac{1}{R^{2\Delta}}\frac{g\left(\zeta\right)}{\left[\left(1-\left(\frac{\vec{r_{1}}}{R}\right)^{2}\right)\left(1-\left(\frac{\vec{r}_{2}}{R}\right)^{2}\right)\right]^{\Delta}}. \tag{5.5}$$

Recall we may plot the two point functions for several values of $\vec{r}_{1}$ and $\vec{r}_{2}$ that have the same cross ratio ζ. If we obtain, for these different configurations, the same value for $g\left(\zeta\right)$,then, this is a strong indication that we have indeed conformal invariance in the three dimensional Ising model. Let us just note that, without imposing inversion symmetry, the dependence of the two point function on the arguments $\vec{r}_{1}$

and $\vec{r}_2$ is slightly more involved.

There are two interesting limits that can be taken in the function $g(\zeta)$. They correspond to the cases in which the two points, $\vec{r}_1$ and $\vec{r}_2$, are coming close together and the limit in which the points are approaching the boundary. In the first case, the leading term to $g(\zeta)$ corresponds to the bulk OPE limit, which can be predicted having information about the anomalous dimensions of the bulk operators. The second limit corresponds to the bulk-to-boundary OPE and the leading term can be determined from the lowest dimension boundary operators. In fig.(5.3a) and fig. (5.3b) we can check these features for both $\sigma(x)$ and $\epsilon(x)$ two point functions, respectively.

As can be seen for the two point function of σ ,in the limit of large ζ, the function can be well approximated by the leading contribution from the bulk OPE. The opposite limit corresponds to the boundary OPE and the leading contribution can be estimated using the results for the dimension of the boundary OPE. Another property that can be seen is that the data seems to be falling on just one curve. Recall that using conformal symmetry, different configurations of the positions $\vec{r}_1$ and $\vec{r_2}$ with the same value of ζ should give the same result. Notice that there is a significant dispersion of the data points on the two point function of the operator $\epsilon(x)$ for small value of ζ, because of lack of statistics.

Chapter 6

Conclusions and future work

One of the primary goals of this work was to be able to implement the known to access the critical region of a statistical system. Along the way, we had the opportunity to understand more several subtleties that stay outside the scope of a generic computational course. We have checked the critical Ising model exponents and the critical temperature both for the 2D and 3D case. For this purpose, we have used finite size scaling and other techniques, such as the Binder's cumulant. We have also observed a strong evidence for the conformality of the 3D Ising model. Using the results of the one and two point functions for the critical Ising model with a spherical boundary, we were able to check dimensions of operators.

For future directions, we could try to measure three point functions in the three dimensional Ising model and compare with the predictions coming from the conformal bootstrap approach. We could also try to get more statistics in several simulations we have performed that would enable to reduce the error in the estimates. We could also try to study other models that have a second phase transition and check if they have conformal invariance.

Bibliography

[1] V. Ambegaokar and M. Troyer. Estimating errors reliably in Monte Carlo simulations of the Ehrenfest model. *American Journal of Physics*, 78:150–157, February 2010.

[2] S. M. Bhattacharjee and A. Khare. Fifty Years of the Exact Solution of the Two-Dimensional Ising Model by Onsager. *eprint arXiv:cond-mat/9511003*, November 1995.

[3] K Binder. Critical properties from monte carlo coarse graining and renormalization. *Physical Review Letters*, 47(9):693, 1981.

[4] James J Binney, NJ Dowrick, AJ Fisher, and M Newman. *The theory of critical phenomena: an introduction to the renormalization group*. Oxford University Press, Inc., 1992.

[5] John Cardy. *Scaling and renormalization in statistical physics*, volume 5. Cambridge University Press, 1996.

[6] Tony F. Chan, Gene H. Golub, and Randall J. LeVeque. Algorithms for computing the sample variance: Analysis and recommendations. *The American Statistician*, 37(3):pp. 242–247, 1983.

[7] Paul D Coddington and Clive F Baillie. Empirical relations between static and dynamic exponents for ising model cluster algorithms. *Physical review letters*, 68(7):962, 1992.

[8] M Dilaver and M Aydin. A study of dynamic finite size scaling behavior of the scaling functions-calculation of dynamic critical index of wolff algorithm. Technical report, 2004.

[9] Sheer El-Showk, Miguel F. Paulos, David Poland, Slava Rychkov, David Simmons-Duffin, et al. Solving the 3D Ising Model with the Conformal Bootstrap. *Phys.Rev.*, D86:025022, 2012.

[10] Sheer El-Showk, Miguel F. Paulos, David Poland, Slava Rychkov, David Simmons-Duffin, et al. Solving the 3d Ising Model with the Conformal Bootstrap II. c-Minimization and Precise Critical Exponents. *J.Stat.Phys.*, xx:xx, 2014.

[11] Alan M. Ferrenberg and D. P. Landau. Critical behavior of the three-dimensional ising model: A high-resolution monte carlo study. *Phys. Rev. B*, 44:5081–5091, Sep 1991.

[12] Hagen Kleinert. Seven loop critical exponents from strong coupling phi**4: Theory in three-dimensions. *Phys.Rev.*, D60:085001, 1999.

[13] David P Landau and Kurt Binder. *A guide to Monte Carlo simulations in statistical physics*. Cambridge university press, 2009.

[14] Nicholas Metropolis, Arianna W Rosenbluth, Marshall N Rosenbluth, Augusta H Teller, and Edward Teller. Equation of state calculations by fast computing machines. *The journal of chemical physics*, 21(6):1087–1092, 1953.

[15] Christian Münkel, Dieter W Heermann, Joan Adler, Misha Gofman, and Dietrich Stauffer. The dynamical critical exponent of the two-, three-and five-dimensional kinetic ising model. *Physica A: Statistical Mechanics and its Applications*, 193(3):540–552, 1993.

[16] MEJ Newman and GT Barkema. Monte carlo methods in statistical physics. 1999.

[17] MP Nightingale and HWJ Blöte. Dynamic exponent of the two-dimensional ising model and monte carlo computation of the subdominant eigenvalue of the stochastic matrix. *Physical review letters*, 76(24):4548, 1996.

[18] Andrea Pelissetto and Ettore Vicari. Critical phenomena and renormalization-group theory. *Physics Reports*, 368(6):549–727, 2002.

[19] Riccardo Rattazzi, Vyacheslav S. Rychkov, Erik Tonni, and Alessandro Vichi. Bounding scalar operator dimensions in 4D CFT. *JHEP*, 0812:031, 2008.

[20] H Eugene Stanley. Introduction to phase transitions and critical phenomena. *Introduction to Phase Transitions and Critical Phenomena, by H Eugene Stanley, pp. 336. Foreword by H Eugene Stanley. Oxford University Press, Jul 1987. ISBN-10: 0195053168. ISBN-13: 9780195053166*, 1, 1987.

[21] Robert H Swendsen and Jian-Sheng Wang. Nonuniversal critical dynamics in monte carlo simulations. *Physical review letters*, 58(2):86, 1987.

[22] Ulli Wolff. Collective monte carlo updating for spin systems. *Physical Review Letters*, 62(4):361, 1989.

[23] Julia M Yeomans. *Statistical mechanics of phase transitions*. Oxford University Press, 1992.

[24] Peter Young. Jackknife and bootstrap resampling methods in statistical analysis to correct for bias. *Statistical Science*, 11:189–228, 1996.